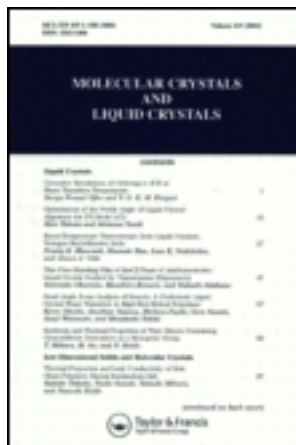


This article was downloaded by: [Tomsk State University of Control Systems and Radio]

On: 19 February 2013, At: 12:41

Publisher: Taylor & Francis

Informa Ltd Registered in England and Wales Registered Number: 1072954
Registered office: Mortimer House, 37-41 Mortimer Street, London W1T 3JH, UK



Molecular Crystals and Liquid Crystals Incorporating Nonlinear Optics

Publication details, including instructions for authors and subscription information:

<http://www.tandfonline.com/loi/gmcl17>

Ferroelectric Liquid Crystals. Material Properties and Applications

K. Skarp^a & M. A. Handschy^b

^a Physics Department, Chalmers University of Technology, S-412 96, Göteborg, Sweden

^b Displaytech, Incorporated, 2200 Central Avenue, Suite A, Boulder, CO, 80301, USA

Version of record first published: 03 Jan 2007.

To cite this article: K. Skarp & M. A. Handschy (1988): Ferroelectric Liquid Crystals. Material Properties and Applications, *Molecular Crystals and Liquid Crystals Incorporating Nonlinear Optics*, 165:1, 439-509

To link to this article: <http://dx.doi.org/10.1080/00268948808082210>

PLEASE SCROLL DOWN FOR ARTICLE

Full terms and conditions of use: <http://www.tandfonline.com/page/terms-and-conditions>

This article may be used for research, teaching, and private study purposes. Any substantial or systematic reproduction, redistribution, reselling, loan, sub-licensing, systematic supply, or distribution in any form to anyone is expressly forbidden.

The publisher does not give any warranty express or implied or make any representation that the contents will be complete or accurate or up to date. The accuracy of any instructions, formulae, and drug doses should

be independently verified with primary sources. The publisher shall not be liable for any loss, actions, claims, proceedings, demand, or costs or damages whatsoever or howsoever caused arising directly or indirectly in connection with or arising out of the use of this material.

Mol. Cryst. Liq. Cryst., 1988, Vol. 165, pp. 439–509
Reprints available directly from the publisher
Photocopying permitted by license only
© 1988 Gordon and Breach Science Publishers S.A.
Printed in the United States of America

Ferroelectric Liquid Crystals. Material Properties and Applications

K. SKARP

*Physics Department, Chalmers University of Technology, S-412 96 Göteborg
Sweden*

and

M. A. HANDSCHY

*Displaytech, Incorporated, 2200 Central Avenue, Suite A, Boulder, CO 80301,
USA*

(Received April 15, 1988)

INTRODUCTION

The last decade has seen a tremendous growth in the research and development activities in the area of ferroelectric liquid crystals. The field was opened up by the work of Meyer in 1974,¹ and has now grown rapidly into one of the major research areas in liquid crystal science. The emphasis of the earlier work was on basic material characterization and phenomenology. Only very few liquid crystalline compounds exhibiting a ferroelectric phase were known at that time, and furthermore these Schiff-base organic compounds were chemically and thermally unstable and presented their ferroelectricity only at elevated temperatures. After the work by Clark and Lagerwall in 1980² on a fast electro-optic effect in a surface-stabilized ferroelectric liquid crystal (SSFLC) structure, both basic and applied research have accelerated, and today a great number of papers deal with development and characterization of ferroelectric compounds and mixtures and various aspects of device physics and manufacturing. It is of some

interest in the present review to try to quantify this growth by plotting the number of research papers per year versus year. Such a plot is shown in Figure 1, where the development in solid state ferroelectrics is also shown.

Extensive chemical work on the synthesis of new, chemically stable ferroelectric smectic compounds and mixtures has recently yielded useful materials for a variety of applications and devices. Basic physical problems of significant current interest are the Landau type description for the smectic A–smectic C transition and the switching mechanisms and states. It might be anticipated that the development of other fundamental areas such as a proper continuum mechanical description of the ferroelectric smectic phases, corresponding to the successful Leslie-Ericksen nematic theory, and applications of the method of molecular dynamics computer simulations to these phases, will be significant over the next few years.

Concentrating on the application potential of these new materials, the present paper attempts to cover some of the important achievements in the format of a short review. Since the subject is very broad, ranging from chemistry, crystallography, optics, physics and electronics to device aspects, it is necessary to be quite selective about what to include. Our aim is to emphasize phenomenology, material characterization and properties of relevance for applications, rather

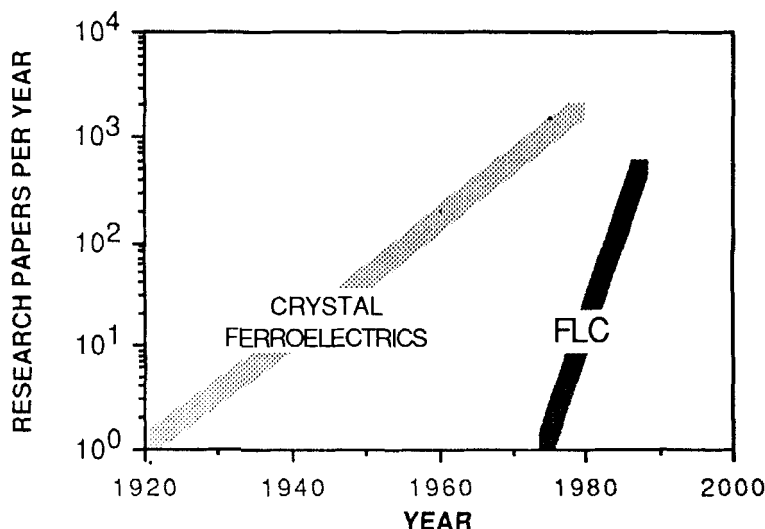


FIGURE 1 Number of research papers on solid state ferroelectrics (dotted line) and ferroelectric liquid crystals (full line) in each year.

than trying to be exhaustive on the physico-chemical and molecular aspects of ferroelectric liquid crystals. An introductory section is devoted to the ferroelectric smectic phases, focussing on the structural properties of the smectic C* phase. The larger section on macroscopic phenomenology deals with the experimental tools for studying ferroelectric liquid crystals and discusses basic phenomena encountered in such studies. Topics of great current interest such as the soft-mode ferroelectric effect, the smectic C* rotational viscosities and the dielectric properties are covered in some detail together with more conventional subjects like the spontaneous polarization and the helical pitch. Theoretical attempts, employing a Landau free energy expansion, to obtain a coherent picture of the thermodynamics of the macroscopic parameters are mentioned in the concluding section dealing with fundamental phenomenology.

The second part of the paper covers the basics of ferroelectric liquid crystal device physics and implementations. The principles for SSFLC electro-optics are given, with emphases on director structures and responses. Linear and matrix arrays, as well as optical shutters and modulators, exemplify the large variety of FLC applications currently under investigation. The review is concluded with a section on optical computing applications of ferroelectric liquid crystals.

MATERIAL PROPERTIES

The Ferroelectric smectic phases

It is generally known in solid state physics that some dielectrics exhibit the property that a nonzero and permanent value of electric polarization, known as spontaneous polarization, exists in the absence of an applied field or stress. Such dielectrics are termed polar materials. If furthermore the direction of spontaneous polarization can be changed by an applied electric field, the name *ferroelectric* is used to denote this sub-class of polar materials. The term ferroelectric is derived from analogy with ferromagnetic materials in that both types of materials possess domains, exhibit hysteresis loops and show Curie-Weiss behavior near their phase transition temperatures.

Ferroelectricity in solid crystals has been known since 1921, when a Rochelle salt was discovered to exhibit dielectric hysteresis indicating a spontaneous electrical polarization. Ferroelectricity in liquid crystals was first demonstrated in 1975 in a paper by the physicist R. B. Meyer together with the chemists L. Liébert, L. Strzelecki and P.

Keller.¹ They were able to show the presence of a spontaneous polarization by investigating the behavior of DOBAMBC (decyloxybenzylideneaniline methylbutyl cinnamate), a material synthesized *ad hoc* to exhibit the above-mentioned properties in having a C^* phase. DOBAMBC has become a classic material in the field of ferroelectric liquid crystals, dealt with in numerous papers since then.

Chiral and non-chiral tilted smectic phases. A significant development in recent years is the smectic classification scheme according to miscibility classes.³ Out of the existing 12 such smectic miscibility classes, seven classes (C, I, F, G, H, J, and K) are characterized by a temperature-dependent tilt $\theta(T)$ between the director and the normal to the smectic layers. If additionally the constituent molecules are chiral (thus exhibiting optical activity), these smectic phases are denoted C^* , I^* , F^* , G^* , H^* , J^* , and K^* . Generally, the 10 crystal classes exhibiting a symmetry that permits a spontaneous polarization belong to the polar point groups C_1 (triclinic), C_4 and C_{4v} (tetragonal), C_6 and C_{6v} (hexagonal), C_2 and C_s (monoclinic), C_{2v} (orthorhombic) and finally C_3 and C_{3v} (trigonal). Examination of the point groups of the chiral tilted smectic liquid crystal phases reveals that C^* , I^* , F^* , G^* , H^* , J^* and K^* , all of which belong to point group C_2 , have the necessary properties to allow for a spontaneous polarization. Hence, all these phases, shown schematically in Figure 2, are ferroelectric. It should be pointed out that the classification of the liquid crystal phases according to point groups is based on the time-averaged local symmetry of the phase in question. It should also be mentioned that regarding the smectic phases only the local symmetry (one layer) has been considered and no attention has been paid to the normally present helicoidal structures of the C^* , F^* and I^* phases. This means that the spontaneous polarization of these three phases is only a local property of each layer and that it is globally averaged to zero as the direction of the polarization changes with the helix. Although C^* , F^* and I^* normally have a helicoidal structure this is not necessarily the case, even in a pure compound. There are two kinds of molecular interactions involved in the helix formation. These give rise to two different effects: a spontaneous twist which is due to the molecular chirality and a spontaneous bend which is a result of the polar symmetry. These effects may act in opposite senses and thus, in principle, a ground state helix-free C^* (or F^* and I^*) can form (in a more or less narrow temperature interval) without a compensation of the polarization. Helix-compensation in mixtures with non-vanishing P has been reported,⁴ and today forms one of several requirements on ferroelectric smectic C^* mixtures for applications.








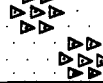



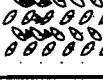


		smectic C*	Random molecular packing. No layer correlation. Short-range in-plane correlation. Molecules tilted. Helix structure.
		smectic I*	Pseudo-hexagonal molecular packing. No layer correlation. Possibly long-range in-plane correlation. Molecules tilted to apex. Helix structure.
		smectic F*	Pseudo-hexagonal molecular packing. No layer correlation. Short-range in-plane correlation. Molecules tilted to side. Helix structure.
		smectic J*	Pseudo-hexagonal molecular packing. Long-range layer correlation. Long-range in-plane correlation. Molecules tilted to apex. No helix structure.
		smectic G*	Pseudo-hexagonal molecular packing. Long-range layer correlation. Long-range in-plane correlation. Molecules tilted to side. No helix structure.
		smectic K*	Herringbone molecular packing. Long-range layer correlation. Long-range in-plane correlation. Molecules tilted to side. No helix structure.
		smectic H*	Herringbone molecular packing. Long-range layer correlation. Long-range in-plane correlation. Molecules tilted to side. No helix structure.

FIGURE 2 The seven tilted smectic phases C, I, F, G, H, J, and K. The corresponding chiral phases C*, I*, F*, G*, H*, J*, and K* exhibit ferroelectricity. Some of them (C*, I*, and F*) develop a helicoidal director structure as their ground state, while in the crystal variants G*, H*, J*, and K* the helix seems to be suppressed (From Ref. 3).

Ferroelectric smectic C compounds and mixtures.* The synthesis of new families of chiral and non-chiral tilted smectics is a major driving force in the whole field of ferroelectric liquid crystals, and several hundred substances exhibiting one or more ferroelectric smectic phases have been reported. A complete coverage of new materials would therefore in principle require a separate review. Hence, we merely specify some prominent synthetic achievements made in the last years, referring to the original literature for further chemical detail. As already mentioned, the first-generation Schiff-base materials, such as DOBAMBC, HOBACPC and the MORA- and MBRA series, did not satisfy basic requirements of chemical and thermal stability. In Table I we summarize some recently reported molecular structures with potential usefulness in mixtures for applications.

TABLE I

Some novel molecular structures of potential usefulness in FLC mixtures. (a) Note. The cited value for the spontaneous polarization is for a doped C*-system with this substance as chiral dopant.

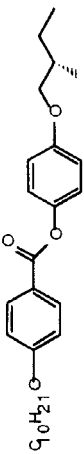
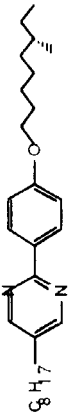
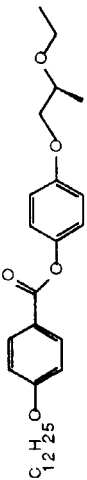
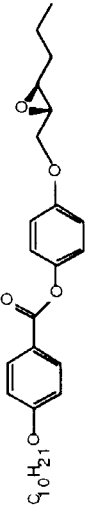
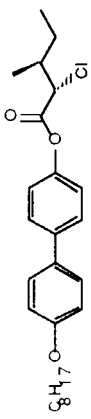
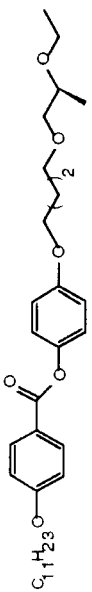
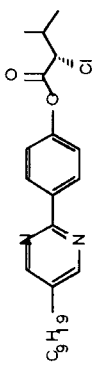
	Phase transitions (°C)	P (nC/cm ²)	[Ref]
	X 44 C* 53.8 A 67 L	3	[76]
	X 3 S _X 14.2 C* 48.6 A 56.3 L	0.5	[77]
	X 44 (34.8 C*) A 46 L	10	[78]
	X 75 (57 S ₃) C* 80 A 81 N* 97 L	30	[79]

TABLE I (continued)

	X 30 C* 53 A 66 L	220	[80]
	X 32 (B 31.2) C* 45.3 A 50.9 L	4	[31]
	C* 71 A 77 N* 94 L	14.3	[81] (a)

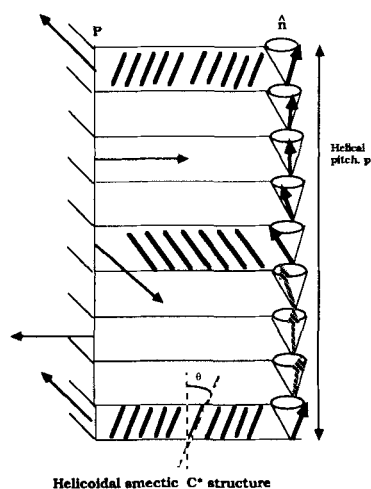
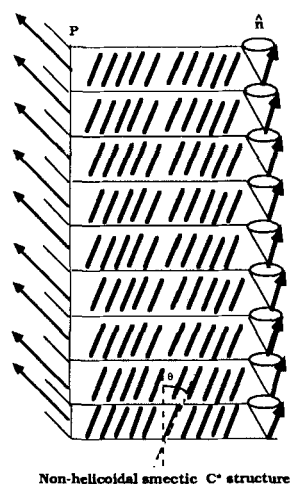
The development of multi-component mixtures is a prerequisite for the production of FLC materials that can be technically useful. For the realization of broad range FLC-mixtures, one may essentially use one of two different approaches. The most conventional one, analogous to the method of developing commercial nematic mixtures, is to use only or at least mainly smectic C*-substances in the mixtures. The other approach is to dope a non-chiral smectic C-mixture with suitable chiral dopants to induce a smectic C* phase. Disadvantages of the first solution are higher viscosities of chiral compounds because of the branched chain compared to non-branched systems. Additionally, chiral compounds are more expensive. In the second concept we have to optimize a non-chiral smectic C-mixture with a low viscosity and also consider the effect of the chiral dopants on the transition temperatures, on the spontaneous polarization and on the switching time of the resulting smectic C*-mixture. Examples of commercial mixtures in general use are CS-1011 from Chisso, ZLI-3488 from Merck and SCE-4 from BDH.

Structure of the smectic C phase.* From an experimental point of view, it is in general necessary for the evaluation of material parameters to have a model for the structure of the sample. Such a model might be introduced on different levels: First it is necessary to discuss the physical properties in terms of macroscopically averaged quantities that are defined in the framework of a phenomenological theory. In the case of the chiral smectic C phase, the notations and ideas are often taken from statistical and dynamical descriptions of nematics. We use the notion of a "nematic-like description" in order to emphasize this situation. A more complete, thermodynamic description, like the hydrodynamic description for nematics, is not yet established for the case of chiral smectics.

Referring to Figures 3a and 3b, one might consider the molecules in the smectic C* phase to form a layered structure, the thickness of one layer being typically of the order 20–30 Å. From X-ray studies one concludes that the molecular centers are packed in a random way within the layers. The molecules tilt from the layer normal by the angle θ . As for nematics the average direction of the molecular long axis is denoted the director, \mathbf{n} . The spontaneous polarization \mathbf{P} is given by

$$\mathbf{P} = P_0 \mathbf{z} \times \mathbf{n} \quad (1)$$

As for most liquid crystalline phases, the variation in space of the vectors characterizing the structure at hand might be extremely com-

FIGURE 3a Helicoidal smectic C^* structure.FIGURE 3b Non-helicoidal smectic C^* structure.

plicated in a general case. For the object of studying physical parameters like dielectric constants and refractive indices, as well as the spontaneous polarization \mathbf{P} , and pitch \mathbf{Z} , it is of great importance to work with well-aligned samples in simple geometries. Two important limiting cases with the layer normal uniform in the sample are shown in Figure 3. In Figure 3a the director spirals on a cone when moving in the z -direction so that a helicoidal structure with a characteristic pitch \mathbf{Z} is formed. This structure is the “natural” one for the chiral smectic C phase, and is adopted when the liquid crystal is free from influences of body forces, external fields or surface conditions. The geometry in Figure 3a is mostly used in helical pitch measurements, although also dielectric measurements have been performed in this geometry. In Figure 3b we illustrate the case when the helix is absent.

To establish the relative direction of the spontaneous polarization, consider one isolated layer of a C^* phase. The C^* phase belongs to the point group C_2 and consequently possesses a two-fold axis of rotation as its sole symmetry element. If the symmetry operation (rotation around the C_2 -axis) is applied to the medium, we can deduce that the polarization vector, \mathbf{P} , can have a non-vanishing component only in the direction of the C_2 -axis, *i.e.* perpendicular to the direction of the tilt and to the director, \mathbf{n} , see Figure 4a. This leaves us with two possibilities; the polarization can point in either of the two directions of the C_2 -axis. A distinction between the two situations has to be made in order to permit a complete description of the material

properties. According to the convention of Clark and Lagerwall,⁶ if \mathbf{z} , \mathbf{n} and \mathbf{P} form a right-handed system the polarization is positive, should they form a left-handed system it is negative, cf. Figure 4b. From this discussion we can also conclude that the molecular contributions adding up to \mathbf{P} are the dipole components directed along the C_2 -axis.

For spontaneous polarization measurements, one might unwind the helix by a sufficiently large electric field, thereby orienting all dipoles and creating a structure with uniform \mathbf{P} (and \mathbf{n}). In this situation also θ can be measured. Alternatively, the boundary conditions of the cell are such that the helix is suppressed by surface stabilization (SSFLC-cell), as already discussed above. In the simplest type of such a cell we can have a uniform director and polarization vector also without an applied field.

While the notions of layer normal, tilt angle, optic axis (in the approximation that the C^* -phase can be considered uniaxial), helical pitch, and even the spontaneous polarization, are rather straightforwardly given an intuitive, geometric interpretation, it is more difficult to have such an immediate understanding of the elastic, viscous and dielectric properties of ferroelectric liquid crystals. This is particularly true when size and boundary effects are considered. Sometimes it seems that the "bulk" properties, even for the simple parameters, are impossible-to-reach idealizations, that often function more as guiding lines than giving the ultimate physical description of the phase. One can think of the difficulties encountered when measuring the helical pitch (extreme surface condition sensitivity), the tilt angle (strong electric field dependence near A-C transition where it is interesting to measure it accurately; possibility of layer tilt in samples), the spontaneous polarization (spurious current contributions,

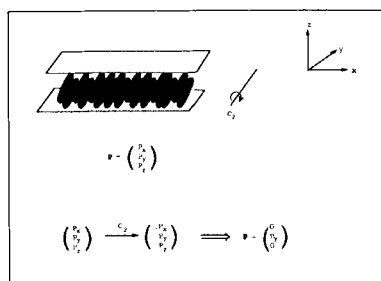


FIGURE 4a C_2 -symmetry operation applied to a single layer C^* (adapted from [5]).

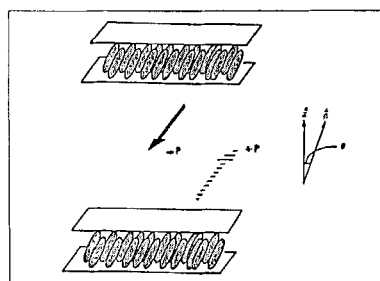


FIGURE 4b The direction of the spontaneous polarization \mathbf{P} .

layer tilt), the dielectric properties (surface condition sensitivity, ionic conduction compensation, high-frequency cut-off in samples), the visco-elastic properties (tentative physical model, complicated experimental evaluation).

Phenomenology

The theoretical concepts usually introduced in the discussion of ferroelectric liquid crystals could be described as being on a macroscopic phenomenological level. The liquid crystal is modelled as a continuum with certain structural and symmetry properties that are specified in terms of continuum variables, *e.g.*, the director $\mathbf{n}(\mathbf{r}, t)$ or the polarization vector $\mathbf{P}(\mathbf{r}, t)$. By different kinds of experiment one may study specific physical properties of these materials, such as the dielectric and optical characteristics. The detailed interpretation of these experiments generally requires an explicit continuum model for the liquid crystal, or at least a macroscopic picture for the origin of the experimentally observable quantities. However, the further step of connecting the physical properties observed on a macroscopic level to molecular parameters is not necessary for understanding ferroelectric liquid crystal devices, since only continuum parameters are used for device modelling. This is true both for device statics (computation of possible equilibrium states and their optical properties) and device dynamics (computation of switching thresholds and dynamics). The continuum concepts used are for example refractive indices, dielectric permittivity, spontaneous ferroelectric polarization, orientational elastic constants and viscosity. Compared to the situation for nematic device modelling, the ferroelectric case represents a greater challenge due to the larger number of continuum parameters and the more complex substrate-liquid crystal interface. Nevertheless, progress in FLC device modelling has been made, ranging from simplified and easy-to-use models to more complete numerical simulations. However, the origin of the macroscopic parameters employed in these simulations can only be understood in terms of the molecular and fluid structure of the liquid. Thus the macroscopic phenomenology forms a bridge between the device physics and the material science of ferroelectric liquid crystals. Consequently, the accurate experimental determination of macroscopic parameters has a two-fold aim: to enable device physicists to model and predict device performance, and to stimulate predictive theories relating macroscopic properties to molecular and fluid structure, thus offering a less empirical approach to the molecular engineering of ferroelectric liq-

uid crystals. In the present section we try to convey the distinctive features of FLC phenomenology and also supply information on the sometimes rather unique experimental methodology that has been developed by several groups for easy and accurate determination of the most important macroscopic parameters.

The most important material parameters from an application point of view, summarized in Table II, are the sign and magnitude of the spontaneous polarization, the tilt angle, the dielectric anisotropy, the refractive indices and birefringence, and the rotational viscosity. From a theoretical point of view also the sign and magnitude of the pitch Z is of great importance, particularly the temperature dependence near the smectic A^* –smectic C^* transition. Many studies have been directed to the measurement of P over the last years, and the experimental methods are now fairly well developed. Therefore our description of the measurement of P is rather extensive. We have also found it relevant to include a discussion on pitch measurements, because of the basic theoretical importance of this parameter. Tilt angle measurements, on the other hand, are usually performed with rather standard optical techniques, so we do not find it necessary to discuss them at length here. Some novel methods for viscosity determinations are discussed. The dielectric properties of ferroelectric liquid crystals are discussed with emphasis on the principally new phenomena encountered in the smectic C^* phase.

TABLE II

The most important macroscopic parameters for the smectic C^* phase.

Ferroelectric polarization	P	(sign and magnitude)
Smectic tilt angle	θ	
Dielectric anisotropy	$\Delta\epsilon$	(sign and magnitude)
Refractive indices	$n_{ }, n_{\perp}$	
Birefringence	Δn	
Rotational viscosity	$\gamma_{\theta}, \gamma_{\phi}$	
Elastic constants	K_1, K_2, K_3	
Helical pitch in C^* phase	Z_{C^*}	(sign and magnitude)
Helical pitch in N^* phase	Z_{N^*}	(sign and magnitude)
Electrical conductivity	σ	
Pyroelectric coefficient	γ	
Surface anchoring coefficients	γ_1, γ_2	

The spontaneous ferroelectric polarization. Values for the spontaneous polarization in solid ferroelectrics typically fall in the 1–100 $\mu\text{C}/\text{cm}^2$ interval, while in smectic C^* liquid crystals values between 1 and 100 nC/cm^2 usually are found in new substances. The polarization value in e.g. DOBAMBC would be close to the cited solid state values if all the molecules were rigidly lined up so that the molecular dipoles could contribute fully to the net macroscopic polarization. Because of the nearly complete rotational freedom around the long molecular axis in the C^* phase, though, usually only a few percent of the maximum values are measured. In phases with a stronger rotational hindrance, such as the smectic I^* or G^* phases, one might expect to find much higher polarization values, but experimental results for these phases are still scarce. The very few cases with ferroelectric polymer liquid crystals studied so far show a spontaneous polarization comparable to low-molecular weight liquid crystals in the C^* phase.⁷

Measurements of the spontaneous polarization are of fundamental importance in the study of ferroelectric smectic liquid crystals. Various methods have been used to measure this quantity, and we will review them shortly in what follows. For routine measurements one often employs polarization switching techniques using an external a.c. electric field, but also pyroelectric methods are in frequent use, especially in the Soviet Union. More occasionally used methods have been shear flow,^{8a} light scattering^{8b} and various indirect methods.

Dielectric versus ferroelectric responses. In the case of ferroelectric smectic liquid crystals, the detailed interpretation of the current responses from externally applied, time-dependent electric fields is still an area of active development. Complicating factors are the dielectric anisotropy, the surface effects and non-uniform director structures, and the conductivity of the samples. In this situation it might be worth while to consider, for a moment, some basic dielectric relations. The relationship between the quantities \mathbf{E} (the electric field vector), \mathbf{D} (the electric displacement vector) and \mathbf{P} (the polarization vector) can be illustrated by referring to the parallel-plate capacitor in Figure 5.

The electric field is a measure of the local field due to all charges, both free and bound, while the displacement \mathbf{D} is a measure only of free charges. The vector \mathbf{P} measures only polarization charges. From electrostatics, the relation between these three vectors are $\mathbf{D} = \epsilon_0 \mathbf{E} + \mathbf{P}$. To the vector \mathbf{P} we can in general have several contributions

$$\mathbf{P} = \mathbf{P}_{\text{ind}} + \mathbf{P}_{\text{perm}} + \mathbf{P}_{\text{ion}} \quad (2)$$

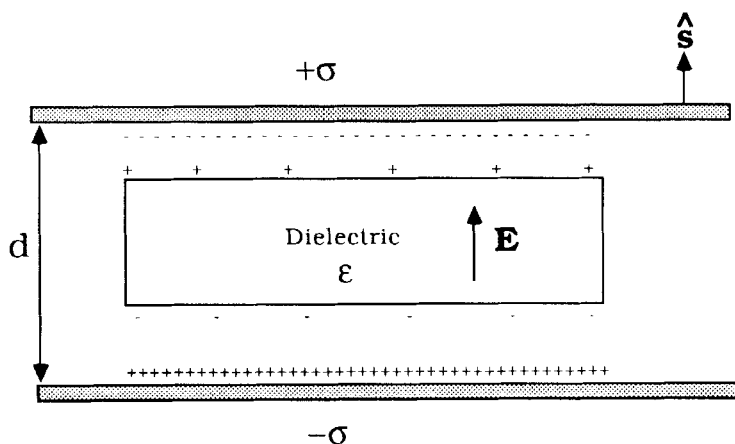


FIGURE 5 Parallel-plate capacitor with a dielectric slab of permittivity ϵ showing free surface charge density $\pm\sigma$ and surface polarization charge density $\pm P$.

where \mathbf{P}_{ind} is the familiar dielectric polarization originating from induced dipole moments. For linear dielectrics we may write

$$\mathbf{P}_{\text{ind}} = \epsilon_0 \chi_\epsilon \cdot \mathbf{E} \quad (3)$$

where ϵ_0 is the permittivity of free space, $\epsilon_0 = 8.85 \cdot 10^{-12}$ F/m and χ_ϵ is the electric susceptibility tensor. The term \mathbf{P}_{perm} originates from the spontaneous ferroelectric polarization in the smectic C^* phase. The relation between \mathbf{P}_{perm} and \mathbf{E} is in general not explicitly analyzed as for \mathbf{P}_{ind} . (In the case of solid ferroelectrics, a critical expansion of \mathbf{E} is often used to model the hysteresis in the \mathbf{P} - \mathbf{E} curve). The contribution from \mathbf{P}_{ion} comes from bulk charges moving in the applied field, and also possibly from injected surface charges at the electrodes.

The underlying principle for the experimental study of ferroelectric phenomena is now to choose an experimental tool that is sensitive to \mathbf{P}_{perm} , at the same time discriminating influences from other polarization sources such as \mathbf{P}_{ion} and \mathbf{P}_{ind} either by direct "hardware" compensation as in the bridge method, or by "software" compensation in the computer evaluation as in the square wave and triangular wave methods to be described later.

In general, one may characterize the different responses from a dielectric slab by the diagrams in Figure 6. The difficulty we face when studying ferroelectric liquid crystals is the simultaneous presence of strong non-linear dielectric response and ferroelectric polarization response. For example, also in a nematic liquid crystal we can

obtain a dielectric response of the form shown in Figure 6c below. This originates from thresholds in reorientation processes of the director. An example of such a threshold is the familiar Frederiks-transition, that causes a marked reorientation of the director at a certain voltage threshold, which in turn leads to a sudden change in the dielectric constant and thus in the cell capacitance. This produces a change in the slope of the P-E curve.

In an actual switching experiment, it is not difficult to imagine that a hysteresis loop may easily develop from the "pure" dielectric curve in Figure 6c. The creation of disclinations, non-elastic changes of boundary conditions, *etc.*, make for a hysteresis curve to occur. This curve is no sign of spontaneous polarization, though. Also for ferroelectric smectics characteristics like the one in Figure 6c have been evaluated to determine spontaneous polarization.⁹ However, these measurements generally give poor agreement with other methods, and should be avoided as a method for measuring spontaneous polarization. Instead, they might be used to study surface-layer changes during the switching.¹⁰

Polarization switching techniques can be used for measuring the spontaneous polarization for ferroelectric smectics in much the same way that they have been used earlier when studying solid state ferroelectrics.¹¹ However, some complications arise making the detailed interpretation of experimental data generally difficult. First of all, because of ionic conductivity in the liquid crystal, one can get erro-

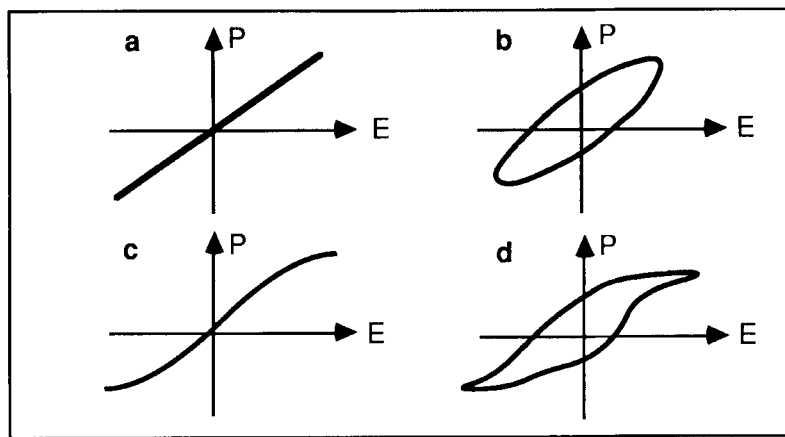


FIGURE 6 P-E responses of different dielectrics. *a.* linear loss-less dielectric *b.* lossy linear dielectric *c.* non-linear loss-less dielectric *d.* non-linear lossy dielectric.

neous responses that are very similar to ferroelectric polarization switching. This is because the characteristic drift velocity of the ions gives a corresponding integrated peak contribution just as the one from polarization switching (and also with the same qualitative electric field dependence). Thus observations, made more than twenty years ago, even led to the conclusion of the existence of a ferroelectric nematic phase.¹² A hysteresis loop was observed also in the isotropic phase, however, and it seems clear now that these effects are connected to the liquid crystal studied being a non-linear lossy dielectric material (in all the fluid phases) rather than a material with spontaneous parallel ordering of the electrical sense of the dipoles. The absence of second harmonic generation is further evidence against a macroscopic dipole ordering in the nematic phase. But, as we pointed out earlier, one nevertheless can observe 'false' hysteresis loops and transient current pulses. The non-linear ionic conductivity and possibly other phenomena (such as active surface layers and electrolytic effects) responsible for this behavior are generally present also when we observe 'true' ferroelectric switching, thereby complicating and distorting these observations.

As a second instance, when comparing liquid crystalline and solid state ferroelectric materials, we might point out the important role that the surface conditions play to establish the static dipole configuration in the case of liquid crystalline ferroelectrics. There is, first of all, the distinction to be made between 'thick' and 'thin' sample cells. In 'thick' cells (thickness of the liquid crystal layer much greater than the helical pitch) the bulk structure with a helix nearly free from distortions is developed. In 'thin' cells, often used in polarization measurements, the cell surfaces induces boundary conditions of more or less complicated nature for the director and the polarization vector. The states occurring during the switching process are then given by balancing surface, electric field, elastic and viscous effects, which generally produces a too complicated mathematical description of the process to be used in a measuring method. Some numerical work has been done in this area,^{13,14} but when relating to an experimental measuring situation one instead would like a simple analytical model that still, however, retains the essential features. We will later mention some recent such models.¹⁵⁻¹⁸ A further complication in the measuring situation is the difficulty to ascertain the orientation of the smectic layers in the cells (they are often tacitly assumed to be perpendicular to the bounding glass plates). It seems today reasonable to assume that much experimental work has been done with cells with different layer tilts. Results from cells with different tilts will

immediately yield systematic but hard to correct errors. For example, the work on DOBAMBC during the last several years, yielding results for P_s between 1 and 10 nC/cm², might well, at least in part, be due to differing layer tilts. Very recent X-ray work has tried to elucidate smectic layer tilt in thin cells,¹⁹ and further work to ascertain knowledge about the smectic layer tilt is certainly needed, also directed to studies on how this tilt might be influenced by the applied electric field during polarization switching.

Ferroelectric hysteresis. In the experimental study of the ferroelectric hysteresis loop one employs variations of the original Sawyer-Tower capacitance bridge set-up.²⁰ The basic circuit is shown in Figure 7 below. The application of a large sine-wave voltage to a linear or non-polar dielectric material results in a current flow which varies sinusoidally with time. By comparison, a typical non-linear or polar dielectric material will have a current flow with contributions from dipolar switching in the material, usually in the form of current peaks. The electrical non-linearity is often displayed as a function of the driving signal rather than as a function of time. This is done using the bridge circuit in Figure 7. An integrating linear capacitor C is placed in series with the polar material. The value of C is chosen to be large enough so that most of the voltage drop in the circuit will

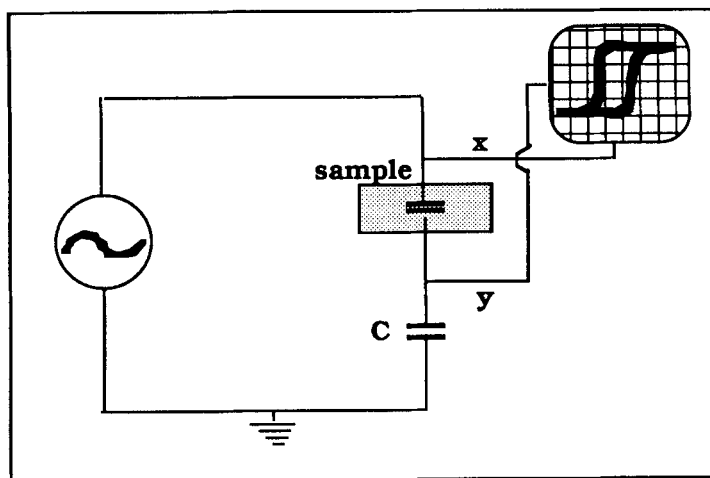


FIGURE 7 The principle for the Sawyer-Tower bridge method for measurement of spontaneous ferroelectric polarization. The capacitor C is a linear dielectric, while the sample forms a non-linear dielectric with capacitance much smaller than the reference C .

occur across the polar material, and thus the voltage at \mathbf{x} is a close approximation to the voltage across the polar dielectric material. The voltage developed across C is

$$U_C = \frac{1}{C} \int i \, dt \quad (4)$$

and hence the voltage at point \mathbf{y} is proportional to the charge q flowing through the polar material. By connecting points \mathbf{x} and \mathbf{y} to the X and Y plates of an oscilloscope one can obtain the q versus V characteristics of the polar dielectric material. Today digital memory oscilloscopes are readily available to record and also evaluate the hysteresis loop.

In order to compensate for the phase shift in the current response signal, one usually introduces a phase compensating circuit, and further one makes the resulting bridge symmetric by introducing another capacitor. Usually also an operational amplifier is employed to act as a high impedance current amplifier. The spontaneous polarization is directly read on the y -axis, as the amplitude of the hysteresis loop is equal to $2P$.

The resulting circuit²¹ shown in Figure 8, can be considered a standard circuit for measuring the spontaneous polarization by the hysteresis method, and is now used in many laboratories for routine measurements on new substances. It is a quick and direct method not requiring computer assistance, and it has a further advantage of being very sensitive (spontaneous polarization values down to 0.01 nC/m^2 can be detected in high-resistivity samples).

Polarization reversal currents. Instead of studying the polarization current as a function of applied electric field, as in the hysteresis loop method, one may alternatively measure the transient current obtained when making a polarization reversal in the sample by changing the polarity of the field. The experimental method involves applying a step function electric field to the sample and measuring the displacement current density $J = dP/dt$ as a function of time. This type of experiment was first carried out on solid state ferroelectrics in 1954²² and was introduced for ferroelectric liquid crystals by Martinot-Lagarde in 1977.²³ It is still probably the most direct method for studying the switching behavior of ferroelectric liquid crystals of low conductivity, and furthermore allows a simultaneous study of the electrical and optical properties during switching. A typical experimental set-up for the square-wave method is shown in Figure 9. The

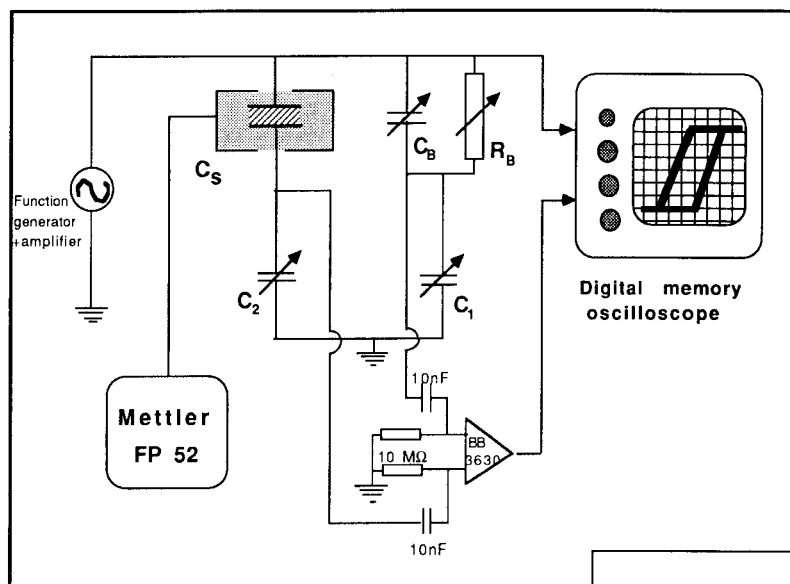
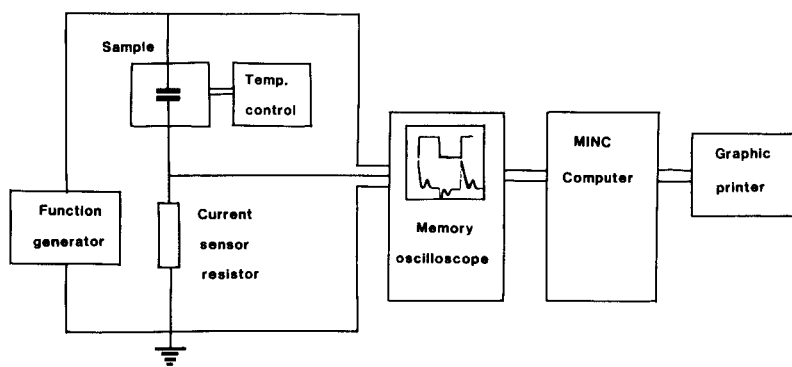


FIGURE 8 A standard measuring bridge for studying the ferroelectric polarization in chiral smectic liquid crystals. A high-voltage amplifier supports the bridge with 0-130V AC voltage in the interval 1 Hz-100 kHz. The sample cell capacitor C_s is balanced by the components C_B and R_B to yield a precisely compensated hysteresis loop.

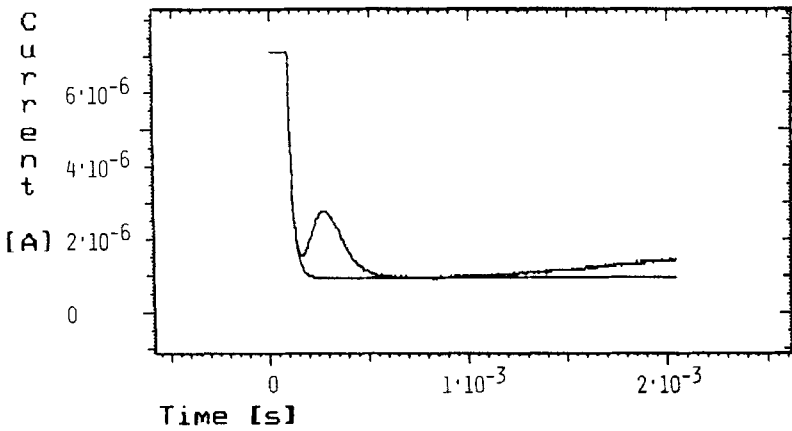


EXPERIMENTAL SET-UP FOR POLARISATION MEASUREMENTS

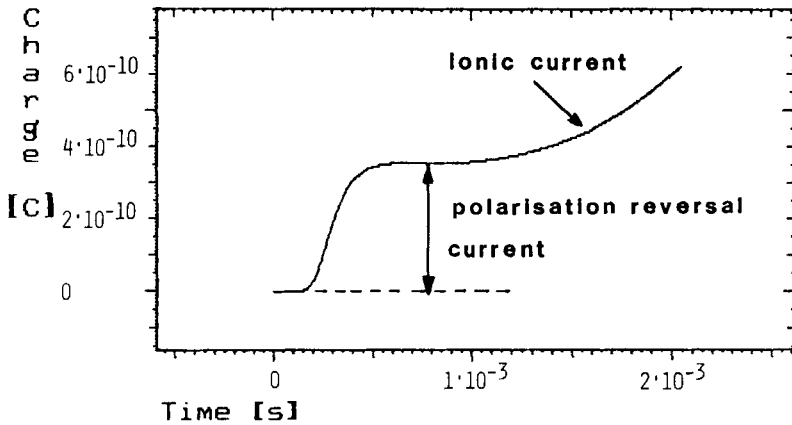
FIGURE 9 A typical polarization reversal experimental set-up.²⁴

square-wave voltage, when applied to the sample, causes a reversal of the dipoles in the ferroelectric liquid crystal. The current associated with this process is measured as the voltage drop over a series resistor, and the signal is read into a memory oscilloscope. Usually the experimental data are transferred to a computer for numerical integration.

The current measured through the sample when applying a voltage step is determined by several factors, as seen in Figure 10. The current



a



b

FIGURE 10 Switching current characteristics with square-wave driving voltage.²⁴

peak due to polarization reversal is usually well separated from the capacitive current (the transient exponential), and also from a conductive current peak often arriving later.

By calculating the area under the polarization current peak, the spontaneous polarization is directly found from the formula

$$P_s = \int i \, dt / 2 A_e \quad (5)$$

where A_e is the actively switching area of the ferroelectric liquid crystal. The problems usually encountered here are how to select the proper background to subtract, and the choice of start and endpoint for the integration. Such problems has led one to construct equivalent circuits for the liquid crystal cell, in order to isolate the ferroelectric component in the current response.²⁴ Another approach is to analyze in more detail the current response in terms of a kinetic model for the switching process. In general, when comparing the results of the hysteresis loop method and the square-wave method on the same ferroelectric sample cell, the agreement is very good. For a few substances we have found that the capability of the square wave method to better separate the current contributions is an advantage, or even in some cases is necessary to be able to perform the polarization measurement. The reason is that the hysteresis loop in such cases is too deformed for a meaningful evaluation. In still other cases, so far for two substances, we have found a good optical switching, indicating a polarization of the order of a few nC/cm², and no disturbing conduction current, but surprisingly seen no trace of the spontaneous polarization in the form of a hysteresis loop, even after several purifications of the compounds.

Excitation by triangular wave voltage. It is possible to produce the polarization reversal by a triangular wave instead of the voltage step described above.²⁵ This method is quite common when studying ferroelectric polymers (e.g., PVDF₂). It has the advantage over the square-wave method of not requiring high-speed switching electronics (in thin cells a rise time of less than one microsecond/100 volt is desired to be able to safely neglect the electric characteristics of the driving electronics). On the other hand the polarization reversal current will be smeared out, leading to some uncertainty when establishing the correct background to subtract before integrating the peak. This uncertainty will especially affect the measured values near the smectic C*–A* transition.

Pyroelectricity in ferroelectric liquid crystals. An attractive possibility to study the ferroelectric polarization in smectic liquid crystals is to take advantage of the temperature dependence of the polarization, especially near phase transitions.²⁶ By heating the liquid crystal sample it is then possible to detect the corresponding polarization current induced by change in net polarization. The existence of this *pyroelectric effect* does not rely on reversibility of polarization. In this sense pyroelectricity is a more general concept than ferroelectricity, where more or less free dipolar rotation is assumed. Materials such as lead titanate and polyvinylfluoride belongs to this more general class of polar dielectrics, and are not ferroelectric. All ferroelectrics are of course pyroelectric and their polarization can be measured by the pyroelectric technique.

The sensitivity of the pyroelectric method is dependent on the magnitude of the pyroelectric coefficient γ

$$\gamma = \frac{dP_s}{dT} \quad (6)$$

which is typically of the order of $10^{-5} \text{ C m}^{-2} \text{ K}^{-1}$ in the case of ferroelectric liquid crystals. The thermal energy needed to induce a temperature rise in the liquid crystal material can be transferred to the sample by several means. Mostly used so far have been the method of dissolving dye molecules in the liquid crystal, with a conveniently placed absorption band for the light source used.²⁶ Alternatively, as in investigations of solid state ferro-electrics, one may deposit a thin heat absorbing layer of, *e.g.*, gold on one of the glass plates in the sample.²⁷

For the experimental determination of the pyroelectric coefficient one generally needs to have a relation between several experimental factors such as the density ρ of the liquid crystal, the heat capacity $c(T)$, an absorption factor η describing the fraction of thermal energy absorbed in the liquid crystal, volt-watt responsivity $S(T)$ and geometrical factors such as the sample thickness d . The basic relation used is

$$\gamma(T) = \frac{S(T) \cdot \rho \cdot c(T) \cdot d}{\eta \cdot R_L} \quad (7)$$

where R_L is a load resistance. The responsivity is the experimentally determined quantity. From the definition of γ we get for the polarization P_s

$$P_s(T) = \int_{T_c}^{T_c - T} \gamma(t) dt + P_s(T_c) \quad (8)$$

where $P_s(T_c)$ is the integration constant ensuring that P_s is zero in the smectic A^* phase above T_c . A typical pyroelectric curve is shown below in Figure 11.

Instead of directly determining the pyroelectric coefficient γ by the measurement of $S(T)$, one may alternatively measure the pyroelectric current

$$i(\omega) = A \gamma \frac{dT}{dt} \quad (9)$$

that is generated as the temperature of the sample is slowly varied. Usually the thermal energy is supplied periodically with a frequency ω from a light source. In the formula A is the electrode area and dT/dt is the rate of heating or cooling of the liquid crystal. If dT/dt , which depends on thermal and geometrical cell factors, is assumed constant, then $i(\omega)$ provides a measure of the relative change of the pyroelectric coefficient as a function of temperature. Integration yields the relative temperature dependence of the spontaneous polarization.

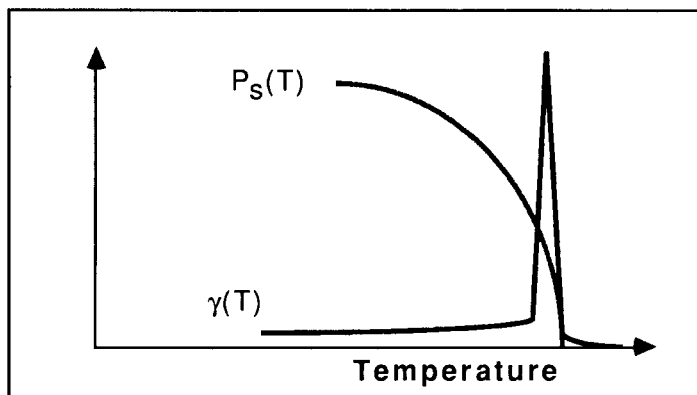


FIGURE 11 Typical experimental curves for the pyroelectric coefficient γ and the calculated polarization P_s .

If absolute values of the polarization are desired, one has to calibrate the measurement at some temperatures by using conventional hysteresis or square-wave techniques.

The soft-mode ferroelectric effect. Pyroelectricity in ferroelectric liquid crystals is only one of several physical effects with great application potential that have been exploited very little so far. In the present section we will describe another potentially useful effect: the soft-mode ferroelectric effect in the smectic A* phase.²⁸ This effect,

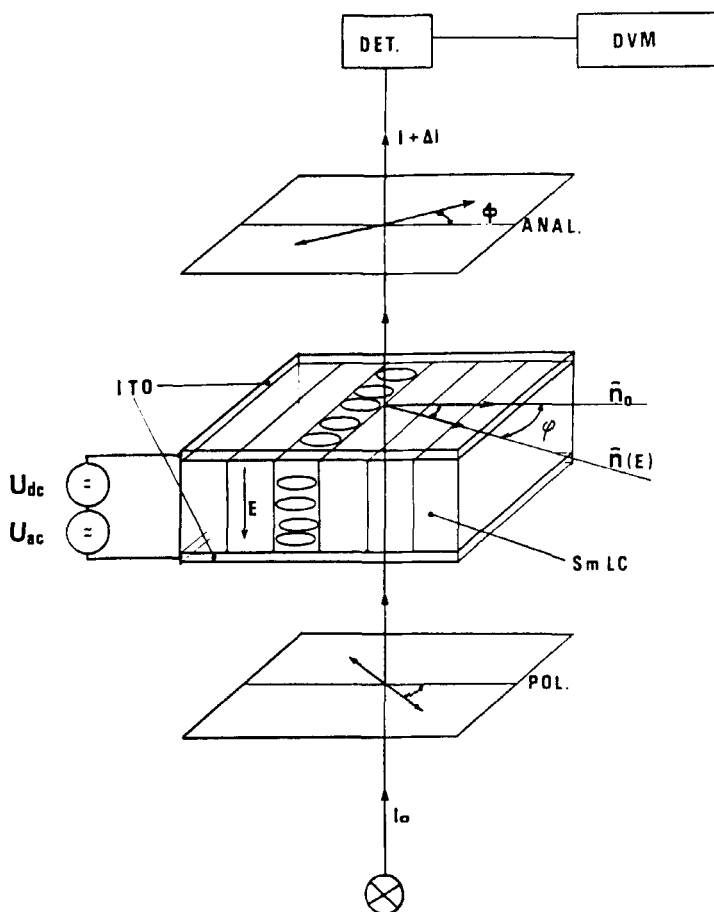


FIGURE 12 Illustration of optic axis changes in "bookshelf geometry" induced by soft-mode switching in the A*-phase. n_0 , n_E -positions of the director without and with field E , respectively; ϕ -angle of rotation of the director due to the electric field.

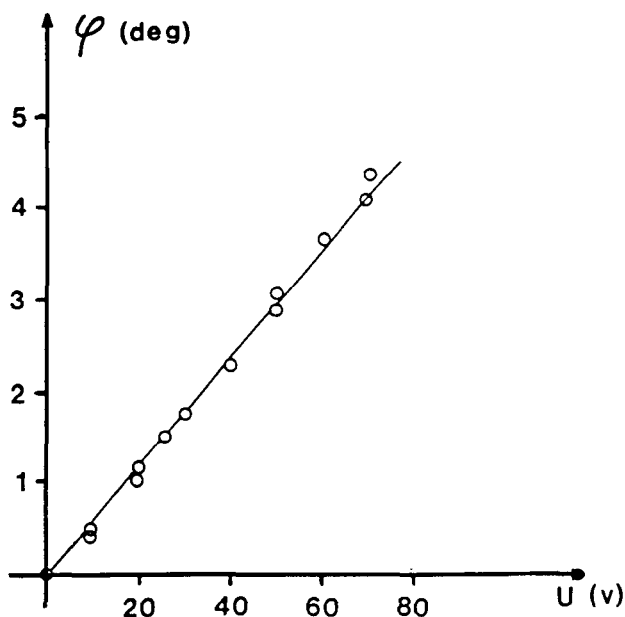


FIGURE 13 Induced tilt angle versus applied voltage in the A^* -phase.²⁸

called the “electroclinic effect” when studied in a thick sample with homeotropic orientation several years ago,²⁹ is now found to be quite general for many studied substances, and also appears in smectic phases other than the A^* phase. It gives a very fast response, for a given substance typically about 100 times faster than the corresponding SSFLC mode at the same applied field.

A convenient set-up for studying the soft-mode switching is shown in Figure 12. The sample is prepared between two ITO coated glass plates with etched electrodes to provide a well-defined switching area. The thickness of the liquid crystal layer is $2\mu\text{m}$, and an excellent bookshelf geometry, indicated in the figure, is obtained by shearing. If an electric field E is applied across the chiral smectic above the C^*-A^* transition, the director will swing out an angle $\varphi(E)$ to the new position of the optic axis. Thus the smectic A^* phase, in this cell geometry, can be considered a retardation plate with a field-sensitive optic axis. In Figure 13 is shown a typical plot of induced tilt angle versus applied voltage. The optical rise times show the general behavior of Figure 14, with the characteristically divergent response times as the A^*-C^* transition is approached. Such behavior is manifested in the corresponding sharp decrease in the relaxation fre-

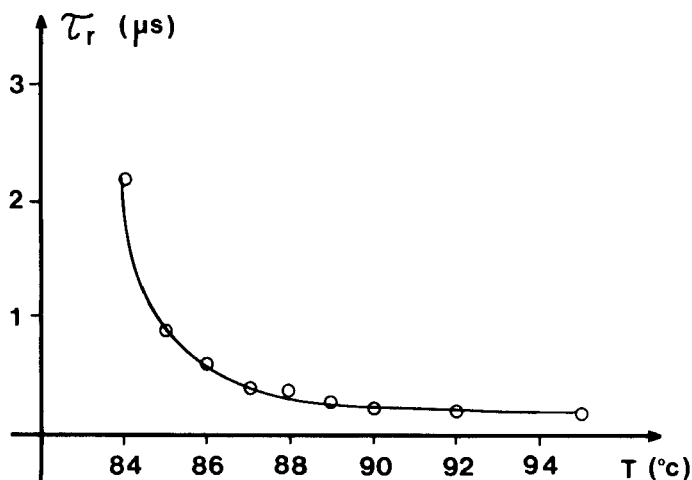


FIGURE 14 Optical rise time as a function of temperature for soft-mode switching in the A^* -phase.²⁸

quency of the soft mode observed in the dielectric studies discussed in a later section.

The soft-mode electro-optic effect can be used in several modes. With a polarizer setting symmetrical with regard to both tilt states there are two different optical extremum states corresponding to field off and maximum applied field, the effect being insensitive to the polarity of the applied field and giving an optical modulation frequency of 2ω if a field of frequency ω is applied. If instead asymmetrical polarizer setting is used, a device with three optical states could be obtained.

Recently, several new compounds have been synthesized, showing larger field induced tilt angles than indicated in Figure 13. The soft-mode switching has also been demonstrated in compounds not exhibiting a C^* phase below the A^* phase, and room-temperature smectic A^* mixtures³⁰ have been prepared in order to facilitate device testing.

The tilt angle. An unambiguous definition of the macroscopic director tilt angle θ is hard to achieve. A primary concern is the different tilt angles obtained when studying a substance with optical methods as compared to, *e.g.*, X-rays determinations. Also the different optical methods for tilt angle determinations sometimes show diverging results. On the other hand, accurate determinations of the tilt angle in various compounds is of great importance in Landau theories of the smectic A – C phase transition, as the tilt angle is

considered to be the primary order parameter driving the smectic A*–smectic C* transition. In one such Landau model, to be described in more detail in a later section, both the tilt angle and the spontaneous polarization are predicted to be proportional to $(T_c - T)^{1/2}$, and thus their ratio should be constant. Experimentally, such behavior is indeed found in several instances, *cf.* Figure 15. In other instances the ratio P/θ shows a drop at the phase transition.

The helical pitch. There are several reasons that a detailed knowledge of the temperature dependence of the helical pitch is of importance. From a theoretical point of view the behavior of the pitch near the smectic C*–smectic A* transition can discriminate between several possible Landau-type descriptions of the smectic C* phase. For applications based on the SSFLC-concept it is important in the display design to have thermal control over the helical pitch.

We will discuss some methods that have been employed for the determination of the helical pitch in the smectic C* phase. The first estimates of the magnitude of the helical pitch were made already by Meyer when demonstrating the ferroelectric properties of DO-BAMBC.¹ In this experiment the focal conic texture, with the smectic layers perpendicular to the glass slides, was observed to contain parallel stripes, that were interpreted to be a direct manifestation of the helicoidal structure in the smectic C* phase. The spacings between the fringes would then correspond to the full pitch for a true bulk

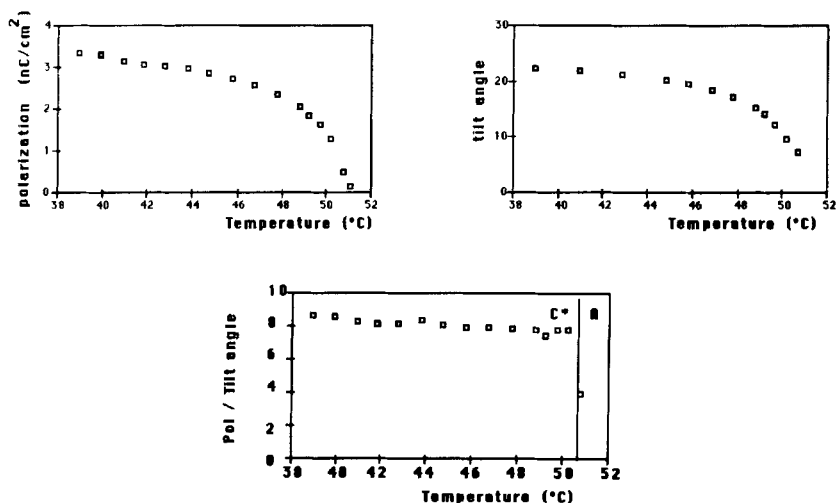


FIGURE 15 Tilt angle, polarization and their ratio as a function of temperature (from Ref. 31).

sample. Since then this direct microscopic method has been used for pitch measurements in many studies.³²⁻⁴² Refinements of the method have involved the use of strong magnetic field or surface coatings for better alignment. An example (for DOBAMBC) with this method is shown in Figure 16 below (from Ref. 35).

The Cano method. A wedge-shaped sample is used in combination with a homeotropic orientation of the smectic liquid crystal (smectic planes parallel to the glass slides). To produce the wedge a lens with known radius of curvature has usually been employed.^{40,43} By proper surface treatment, e.g., with a CTAB surfactant and gentle shearing, it is possible to produce a homeotropic sample with oriented c-director. By observing the successive Cano-disclinations, that divide areas in which the rotation of the c-director differs by 2π , the determination of the helical pitch is possible. A recent result is shown in Figure 17. The interesting result from the observations with this method is that a maximum in the pitch near the smectic C*-smectic A* transition is not observed. This is contrary to measurements by several other methods, and will be discussed below.

Selective reflection. In this method one also uses a homeotropic sample, and studies the selective reflection of light incident perpendicular to the smectic planes. A selective reflection band appears in the smectic C* phase at the wavelength $\lambda = \sqrt{\epsilon} Z$. A complication with the selective reflection method is that it is necessary (for the

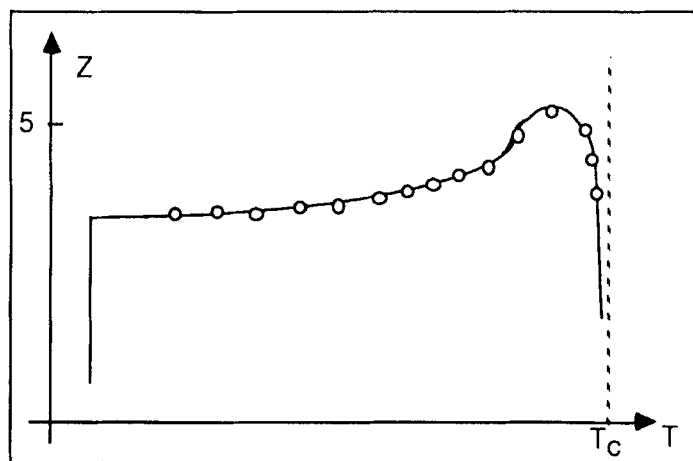


FIGURE 16 Helical pitch by direct microscopical observation (adapted from Ref. 35).

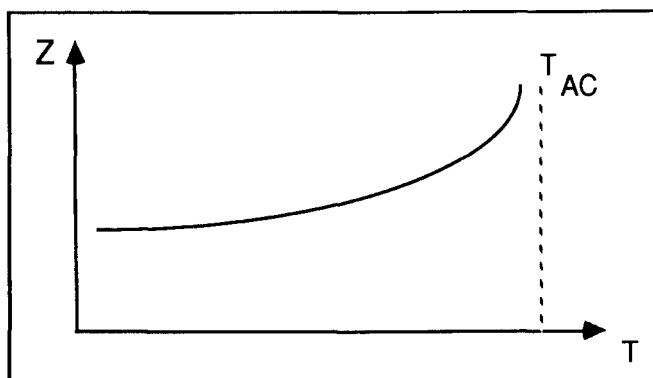


FIGURE 17 Qualitative temperature dependence of the helical pitch obtained by using the Cano method.

calculation of ϵ) to know the tilt angle and the refractive indices by independent measurements for the final determination of the pitch. For the refractive indices, one has taken values in the smectic A phase. The method has been used to establish that with the direct microscopic and diffraction methods really the full pitch is measured.⁴⁵ A problem when using this method is the absorption of the IR-light in the glass slides.⁴³

The diffraction method. Probably the most widely used method for routine measurements of the helical pitch is diffraction of a laser light beam on the periodic helicoidal structure.^{34,45} When using very well oriented samples it is possible to obtain almost point-like diffraction spots, while in many instances one observes more arc-like diffraction patterns, indicating a not completely perfect parallelism in the smectic layer structure. However, such orientation quality is often good enough for pitch measurements. Usually one may observe up to 3rd or 4th order diffraction. The helical pitch Z is determined from the formula $Z = N\lambda[\lambda + (b/a)^2]^{1/2}$ where N is the diffraction order, a is the distance on the screen between the central beam and the N :th order diffraction spot, b is the distance between the sample and the screen and λ is the wavelength of the laser light.

The temperature dependence of the pitch. A question of considerable current theoretical interest is the behavior of the helical pitch near the smectic C*-smectic A* transition. According to classical Landau theory the pitch should be temperature-independent (see later section on thermodynamic models). Experimentally, a strong temperature dependence is found, especially near T_{AC} . With the dif-

fraction and direct microscopic observation methods one has experimentally in the vast majority of cases found a maximum in the pitch near T_{AC} , as in Figure 16, while very recent experiments with the Cano and selective reflection methods yield no such maximum, but instead a very clear divergence at T_{AC} as already described. It has been known for a long time that the helical pitch is extremely sensitive to disturbances from the bounding surfaces, and already at thicknesses of hundred times the helical pitch might this influence be noticeable.⁴⁵ The conclusion from such experiments is that measurements in the "bookshelf" geometry (with the smectic planes perpendicular to the glass slides) using any of the methods described above are likely to give a helical pitch somewhat shifted from the true bulk value. Thus, although recent Landau-theories, by including a bi-quadratic coupling term between P and Z , seem to describe quantitatively the helical pitch behavior near T_{AC} as observed in the bookshelf geometry, the newer observations of a diverging pitch, made in a geometry where the boundary influence is minimal, demonstrates that the theoretical attempts to describe the temperature dependence of the helical pitch using various Landau expansions have to be reconsidered from new premises.

The rotational viscosities. The study of viscosity effects in the smectic phases is in its infancy. The rotational viscosity in the smectic C^* phase is thus not as firmly based on a continuum theoretical description as is the case for the corresponding nematic quantity γ_1 . However, it is always possible to introduce a term of the form

$$\gamma_1 \frac{d\phi}{dt} \quad (10)$$

to describe the viscous torque acting to reduce an existing angular velocity $d\phi/dt$. This is also the way one usually introduces the time-dependence in order to describe dynamical switching in ferroelectric liquid crystal cells.^{13,14,18,46,49} In the nematic case it is today established, through the Leslie-Ericksen continuum description, how this director torque is coupled to other director torques (*e.g.* of surface or external field origin), and also how it in general couples to the velocity field to introduce a flow in the liquid crystal. The present situation for smectic C^* liquid crystals is not equally well developed, but in order to describe, *e.g.*, switching phenomena caused by the application of an external electric field, a description neglecting material flow effects and thus involving only the director equation is

often employed. Moreover, one often studies the smectic far from phase transitions, so that the tilt angle θ is considered constant; further the smectic layers are considered to be parallel. Even with these simplifying assumptions, the continuum description of the smectic C* phase becomes complicated.^{50a}

Scaling rule for the rotational viscosity. Referring to Figure 18 below, let us discuss the rotational viscosity in the smectic C* phase as related to the rotational viscosity in the nematic phase. One model that might be used is to consider the director in the smectic C* phase to be dynamically similar to a nematic director constrained to the cone $\theta = \text{constant}$. By dynamically similar we mean that the smectic c-director will be damped by a viscous torque that is just the z-component of the viscous torque acting on the n-director. The viscous torque on the n-director Γ^n is given from the hydrodynamics of nematics as

$$\Gamma^n = -\dot{\mathbf{n}} \times \gamma_1 \dot{\mathbf{n}} \quad (11)$$

The direction of this torque is such that it always tends to diminish a director angular velocity that has been introduced by, *e.g.*, an

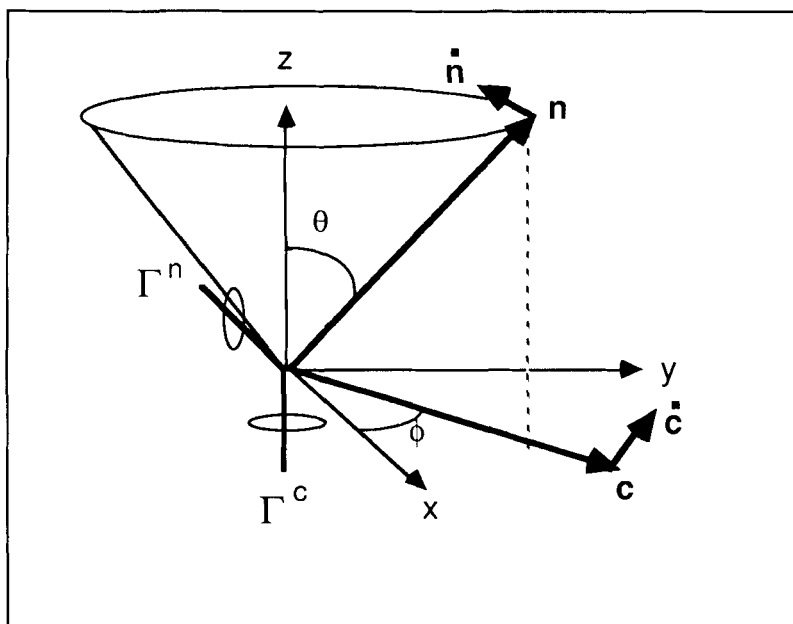


FIGURE 18 Definition of angles and vector notation in the smectic C phase.

application or removal of a shear flow or an external magnetic or electric field. Let us now calculate this torque for the polarly constrained nematic director of Figure 18. The director may be expressed in polar coordinates as

$$\begin{aligned}n_x &= \sin\theta \cos\varphi \\n_y &= \sin\theta \sin\varphi \\n_z &= \cos\theta\end{aligned}\tag{12}$$

The z-component of the torque Γ^n is calculated to be

$$\Gamma_z^n = -\dot{\varphi}\gamma_1 \sin^2\theta\tag{13}$$

If now the viscous torque on the smectic c-director is introduced in formal analogy with the definition of the viscous torque in nematodynamics, we may write

$$\Gamma^c = -\dot{\mathbf{c}} \times \gamma_c \dot{\mathbf{c}}\tag{14}$$

where γ_c is the rotational viscosity for the c-director. The z-component of Γ^c is found to be:

$$\Gamma_z^c = -\gamma_c \dot{\varphi}.\tag{15}$$

If we now compare the expressions for the n-director and the c-director, we can infer the relation

$$\gamma_c = \gamma_1 \sin^2\theta\tag{16}$$

The proportionality of the rotational viscosity γ_c to $\sin^2\theta$ has also been concluded from a molecular statistical model.⁵¹ If $\sin^2\theta$ is taken to be the square of the order parameter in the C* phase, the result of the molecular model is analogous to the nematic case: If the nematic order parameter is S, a scaling factor S² is often used to facilitate comparisons between different compounds.⁵² The experimental material is at present not large enough to enable a verification of the scaling rule given above, although some experiments independently determining γ_1 and θ have been reported.⁵³

One might ask whether a similar theory to the Leslie-Ericksen description for nematics has been developed also for smectic C*.

Some such theories have recently been put forward.^{50a,50b,54} They consider cases when one can neglect distortions of the smectic layers, so that these descriptions are in a way “nematic” descriptions for the smectic \mathbf{c} -director introduced above. One result from these models is that 9 independent viscosities enter the description, compared to 5 in nematodynamics. The notation is analogous to the nematic case, if instead of the \mathbf{n} -director we introduce the \mathbf{c} -director. In addition, we need to introduce a third vector, besides \mathbf{c} and \mathbf{v} , namely the smectic layer normal \mathbf{k} . It is the several possible relative orientations of vectors \mathbf{c} , \mathbf{v} and \mathbf{k} , in combination with different velocity gradients, that accounts for the large number of viscosities for the C-phase. Thus ten terms in the stress tensor, all describing coupling between orientation and flow in the C-phase, are required compared to three terms in the nematic case. Typical consequences of this coupling, such as flow alignment and backflow effects familiar from nematodynamics, thus in principle occur also in the smectic C-phase. However, since backflow effects do not seem to disturb FLC device performance, we will not pursue the discussion of these topics here. Rather we will describe, in a less formal way than so far, rotational viscosities in the nematic, smectic A and smectic C phases, *cf.* Figure 19.

The notion “rotational viscosity”, as used in, *e.g.*, dynamical models for the ferroelectric switching in the C*-phase, refers to the motion on the cone. Only very near to the smectic A phase is the tilt angle supposed to be influenced by the switching field for normal field strengths. On the other hand, in the smectic A phase the relevant coefficient for describing, for example, the soft-mode or electro-clinic switching, is of course γ_θ . Thus, in a temperature region around the A–C transition, both Goldstone-mode (involving γ_ϕ) and soft-mode (involving γ_θ) switching are important, and indeed lead to an intricate switching behavior when both the phase and amplitude of the projection of the director on the smectic plane change during the switching.

Measurements of the rotational viscosity. Measurements of rotational viscosity for nematics have been carried out for a long time using several methods.⁵⁵ The corresponding determinations for smectic phases are much less developed, regarding both the theoretical and the experimental situations. The rotational viscosity, discussed in the previous section, is of obvious importance when studying, *e.g.*, dynamical switching phenomena in different FLC cell configurations. It is only very recently, though, that progress has been made in developing accurate and reasonably simple methods for viscosity de-

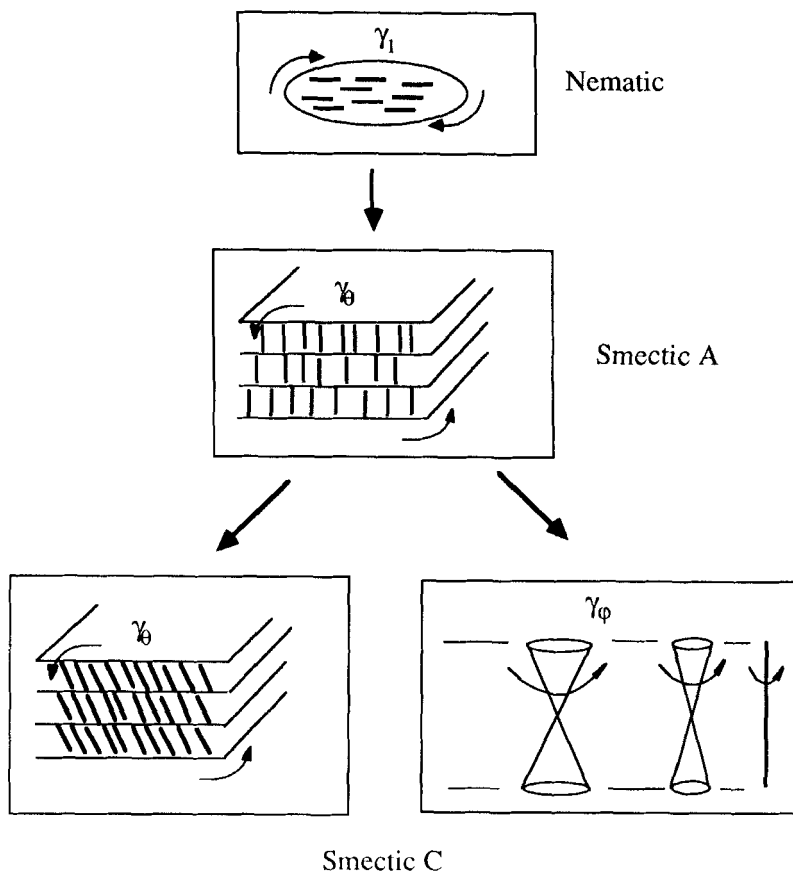


FIGURE 19 The single rotational viscosity in the nematic and smectic A phases will be split into two in the smectic C phase, associated with motion on the cone and tilt-angle variations, respectively.

terminations. Such methods include pyroelectric techniques, electro-optic methods and measurements of the polarization current using square wave or triangular wave driving voltages.

In the first reported measurement of rotational viscosity in a smectic C material⁵⁶ a magnetic field was used to lock the director, and the viscous torque was measured in a torsional pendulum set-up. Results show a drop in viscosity at nematic-smectic C transition, but is otherwise hard to interpret (a combination of two viscosities might be measured). Other mechanical methods giving information on the viscoelastic coefficients involve disturbing of the helix in the smectic C* phase by an alternating shear or Poiseuille flow, and measuring the

current and studying the dynamic conosopic picture.^{57,58} Because of complicated experimental set-ups, these mechanical methods are presently less popular.

The pyroelectric effect has been used for about ten years studying polarization properties in ferroelectric smectics.⁵⁹ More recently, also information about viscosity has been extracted from these measurements.⁶⁰ By using short laser pulses to induce the pyroelectric current and study the transient current decay, one may obtain the γ_θ viscosity. Combining pyroelectric results for γ_θ with electro-optic measurements of γ_φ for the same substance makes a very interesting comparison of the two viscosities possible.⁶¹

The most convenient way for studying the rotational viscosity is to use the same kind of cells as in the SSFLC-configuration. One can then measure the optical response time τ on an applied voltage step,² and estimate the viscosity from the response time. The formula often used for evaluating the viscosity from such measurements is

$$\tau_{10-90} = \frac{\gamma_\varphi}{PE} \quad (17)$$

where the time is measured from 10 to 90 percent transmission between crossed polarizers (cf. Figure 20a).

This formula, assumed to apply for "bulk-switching," has later been given a founding in a calculation of electro-optic switching characteristics,¹⁵ which results in the formula

$$\gamma_\varphi = \frac{1}{1.8} \tau_{10-90} PE \quad (18)$$

being applicable in most cases (the numerical constant depends on dielectric anisotropy). The switching model is made for the region of electric fields (high enough field) where elastic effects can be neglected.

In the method just described, one switches the c-director on the full half-cone (or nearly so), thereby being in a non-linear switching regime (driving torque is $PE \sin \varphi$, where φ takes on values between 0 and π). A less violent method, more in the line of dielectric measurements, is to apply only a small alternating field and study the director deviations from an equilibrium configuration by an optical conosopic method.⁴⁸

Studies of the polarization reversal current in ferroelectric liquid crystals were begun by Martinot-Lagarde.²³ The motivation was to

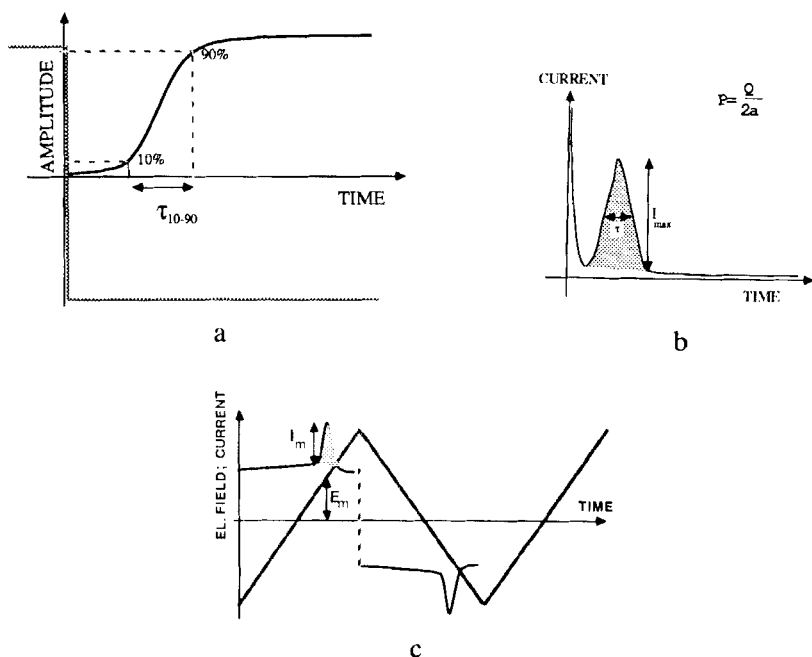


FIGURE 20 *a.* Electro-optical response curve. *b.* Transient current from square-wave driving voltage. *c.* Response from triangular-wave excitation.

evaluate the spontaneous polarization from these experiments, but later attempts were made also to get information for the rotational viscosity. Today, several simplified analytic switching models exist enabling a detailed evaluation of such polarization reversal experiments.

The most important input parameter of relevance for the viscosity is the half-width of the current peak (*cf.* Figure 20b), while the peak's position on the time axes is more complicated to evaluate. For determination of the viscosity one might use the formula for the half-width of the peak

$$\gamma_{\varphi} = \frac{1}{1.8} \tau_w \text{ PE} \quad (19)$$

Refinements include considerations of the elastic (boundary) effects,¹⁶ dielectric torques,¹⁵ fluctuations¹⁷ and layer tilt.⁶² It is now possible to account for asymmetric current peaks with several of these

models, while a proper prediction of the position of the peak on the time axis seems to require consideration of elastic effects.¹⁶

Also the current response on a triangular driving voltage (*cf.* Figure 20c) has been analyzed to yield information on the rotational viscosity.¹⁸ In the current peak one reads the maximum height I_p^m at the electric field E_m and then the viscosity is given by

$$\gamma_\varphi = \frac{A P^2 E_m}{I_p^m} \quad (20)$$

In some cases cell conductivity makes it difficult to properly define a baseline for the current response, causing substantial uncertainty in the viscosity determinations. It is often useful in these instances to also make a measurement using square-wave driving voltage, offering time separation of the conductive current peak.

It is instructive to make a 3D-graph of the time development of the polarization current response on a voltage step at time $t = 0$. Such a plot is shown in Figure 21. The computation is based on a simple switching model, where the polarization vector \mathbf{P} at $t = 0$ is assumed to form a small angle (1° in the curves of Figure 21) to the applied electric field \mathbf{E} . The time evolution is then governed by a torque balance between only two torques: the ferroelectric driving

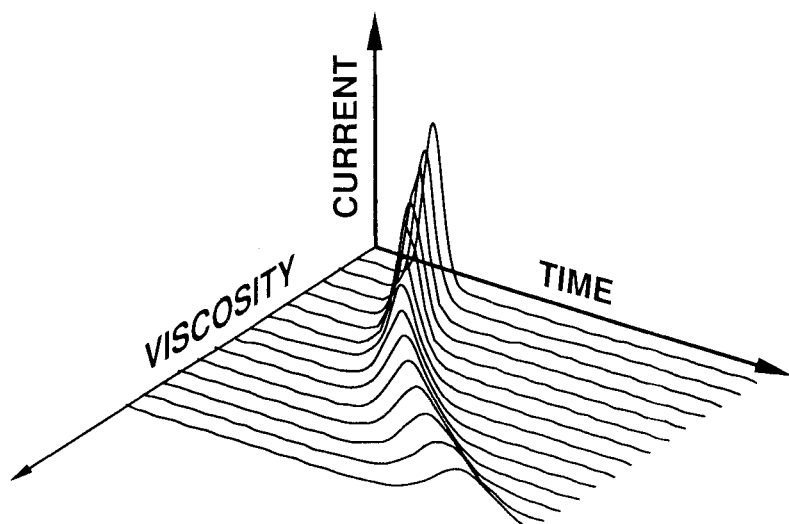


FIGURE 21 Time development of the polarization reversal transient current computed with the rotational viscosity γ_φ as parameter.

torque and the viscous damping torque. Between each curve the rotational viscosity γ_φ is increased by about 10%, so that there is a factor of about 3 in viscosity between the first curve (with the fastest current peak) and the last curve (with the slowest current peak). The area of the peaks, which is proportional to the spontaneous polarization, is constant, while the half-width of the peaks changes with viscosity according to the equation given above for square-wave switching.

Taking the torque balance between the ferroelectric driving torque and the viscous damping torque, the governing equation for the azimuthal angle φ will be

$$\gamma_\varphi \frac{\partial \varphi}{\partial t} = PE \sin \varphi \quad (21)$$

with the solution

$$\frac{t}{\tau} = \ln \frac{\tan \frac{\varphi}{2}}{\tan \frac{\varphi_0}{2}} \quad (22)$$

where $\tau = \gamma_\varphi/PE$ and $\varphi_0 = \varphi(t = 0)$. The polarization reversal current is given by

$$i = \frac{P}{\tau} \sin^2 \varphi \quad (23)$$

or explicitly as a function of time

$$i = \frac{P}{\tau} \sin^2 \left\{ 2 \arctan \left(\tan \frac{\varphi_0}{2} e^{t/\tau} \right) \right\} \quad (24)$$

which gives the reversal current with P , γ_φ and φ_0 as parameters. This formula is used for producing the 3D-graph of Figure 21.

Rotational viscosity and response times. The electro-optic response times are in general determined by a combination of viscosity parameters and other parameters. If we neglect elastic torques on the director, we might easily estimate the importance of these different parameters for the switching times. Starting with a purely dielectric switching, the important field coupling constant is the dielectric anisotropy $\Delta\epsilon$.

The natural times for the equations in Figure 22 (often called bulk switching times) have characteristic field dependences according to the nature of the director torques. For a pure dielectric coupling, the switching time is inversely proportional to E^2 , while in the ferroelectric case it is inversely proportional to E . The third equation describing the soft-mode switching in the smectic A^* phase yields a switching time independent of E .

Concentrating now on a comparison between the ferroelectric and electroclinic switching near the transition, an outline of their temperature dependencies is shown below in Figure 23a. Assumptions for the curves are that the viscosity in the C^* phase is proportional to θ^2 , while the polarization is proportional to θ . In the A^* phase the critical behavior $A = a(T-T_c)^{-1}$ is dominant.

Experimentally it is found that for substances showing a strong softmode response in the A^* phase, the switching time behavior in the transition region deviates from the idealized in Figure 23a. The viscosity γ_θ in the A^* phase can be estimated from the relation $\tau_\theta =$

$\frac{1}{2}\epsilon_a E^2 \sin 2\theta + \gamma_N \frac{d\theta}{dt} = 0$	$\tau_N = \frac{\gamma_N}{\frac{1}{2}\epsilon_a E^2}$
$PE \sin \varphi + \gamma_\varphi \frac{d\varphi}{dt} = 0$	$\tau_\varphi = \frac{\gamma_\varphi}{PE}$
$cE + \gamma_\theta \frac{d\theta}{dt} = A\theta$	$\tau_\theta = \frac{\gamma_\theta}{A}$
$[A=2a(T-T_c)]$	

FIGURE 22 Simplified equations for pure dielectric, ferroelectric and electroclinic torque balance. The natural times in these equations, shown to the right, yield expressions for the response times.

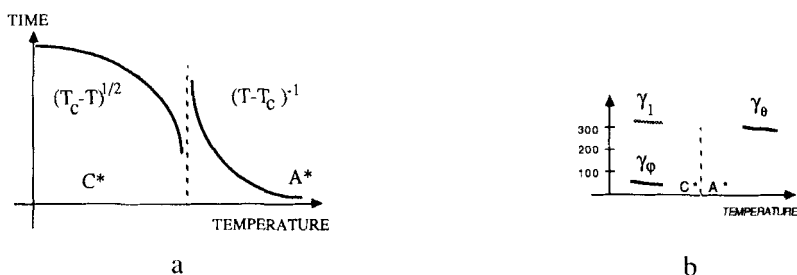


FIGURE 23 *a.* Temperature dependencies for idealized ferroelectric (C^*) and soft-mode (A^*) switching. *b.* Rotational viscosities in the A^* and C^* phases.

γ_θ/A . The thermodynamic coefficient $A = 2a(T-T_c)$ can be supplied from independent measurements of the temperature dependences of the heat capacity and the tilt angle. If thus heat-capacity measurements⁶³ for DOBAMBC, giving $a = 22000 \text{ J/m}^3 \text{ K}$, are combined with recent experimental data for a similar substance with strong soft-mode response, DOBA-1-MPC,²⁸ γ_θ in the smectic A^* phase might be estimated. In the C^* phase γ_ϕ is obtained with the electro-optic response time method described above. For comparison a typical nematic viscosity γ_1 is also shown in Figure 23b. For $\theta = 0.3$, it is found that γ_ϕ scales approximately according to $\gamma_\phi \sim \gamma_\theta \sin^2 \theta$.

The dielectric constants. Dielectric studies of liquid crystals provide valuable information of great interest both from fundamental and applied aspects. For non-chiral liquid crystals, it has been possible to extract some information about the dipolar ordering for the nematic,⁶⁴ smectic A ⁶⁴ and smectic C ⁶⁵ phases. The dielectric relaxation behavior contains interesting indications concerning the possible molecular motions, which are mainly of non-collective type, for instance molecular rotations around the long and short molecular axes. The major technological significance of dielectric studies at present is the importance of the dielectric anisotropy $\Delta\epsilon$ for display applications.

Goldstone mode and soft-mode dielectric contributions. Chiral liquid crystals (especially smectic phases) exhibit a rich variety of fundamental dielectric phenomena, many of them of immediate technological importance. A recent example is the observation of an additional dielectric response in the chiral smectic A phase (the A^* phase) in the perpendicular component of the static dielectric constant ϵ_\perp . This additional contribution $\Delta\epsilon_A$ to the dielectric response is attributed to the distortion of the tilt angle θ , the so-called soft-mode⁶⁶

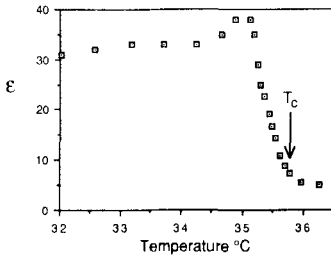


FIGURE 24a Dielectric constant increment in the C* phase.

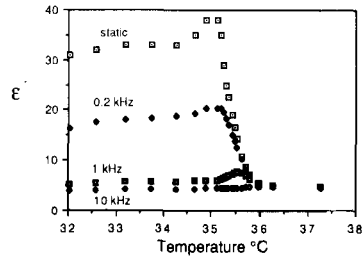


FIGURE 24b Dielectric constant increment in the C* phase for different frequencies.

ferroelectric effect. In the ferroelectric smectic C* phase itself, there are two types of deformations. The first one is the soft-mode—as in the A* phase—and the second one is helix deformation or the deformation connected with the change in azimuthal angle φ , the so-called Goldstone mode.

Using a Landau free energy expansion for the A*–C* transition, the dielectric increment in the A* phase $\Delta\epsilon_{A^*}$ and in the C* phase $\Delta\epsilon_{C^*}$ are given by⁶⁷

$$\Delta\epsilon_{A^*} = 4\pi C^2 \chi^2 / [Kq^2 + \alpha(T-T_c)] \quad (25)$$

$$\Delta\epsilon_{C^*} = 2\pi \{ C^2 \chi^2 / Kq^2 + C^2 \chi^2 / [Kq^2 + 2\alpha(T-T_c)] \} \quad (26)$$

where χ is the high temperature susceptibility, C is a constant which represents the coupling between the spontaneous polarization P and the tilt angle θ , $q = 2\pi/Z$, Z being the pitch of the smectic C* helix, $K = K_{33} - \chi\mu^2$, where K_{33} is the bend elastic constant and μ is the flexoelectric constant. The function $\Delta\epsilon_{C^*}$ given above has its maximum for $T = T_c$ contrary to the typical experimental result shown in Figure 24, which shows a maximum a few tenths of a degree below T_c . Further attempts⁶⁸ have been made to improve the theoretical situation by considering a strong biquadratic interaction between the primary phase transition order parameter and the polarization P . The temperature dependence of the soft-mode response $\Delta\epsilon_{A^*}$ has the form of Curie-Weiss law, but the divergence at T_c is cut off as shown in Figure 25. The Goldstone mode and soft mode dielectric contributions shown in Figures 24 and 25 are two characteristic features in the dielectric behavior of ferroelectric liquid crystals.

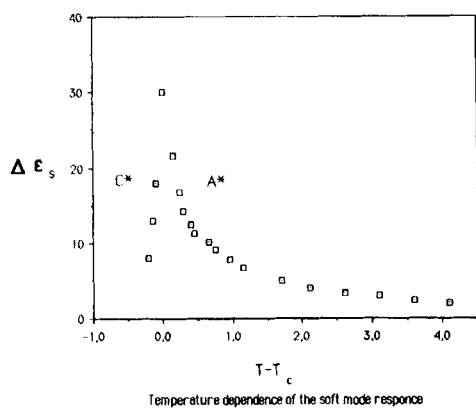


FIGURE 25 Temperature dependence of the soft-mode response.

As already mentioned, the possibility of technical applications of the soft-mode for fast switching has been established.²⁸ The relaxation frequency of the soft-mode f_s , of great significance for device implementations of the soft-mode effect, can be obtained by dielectric measurements.⁶⁹ The temperature dependence of f_s is shown in Figure 26 for a wide temperature range in the smectic A* phase of a high polarization compound ($P_s = 50 \text{ nC/cm}^2$). In the same figure is also shown the relaxation frequency of the Goldstone mode f_G .

To get the real (ϵ') and imaginary (ϵ'') parts of the complex dielectric constant, one has to perform measurements of both the capacitance

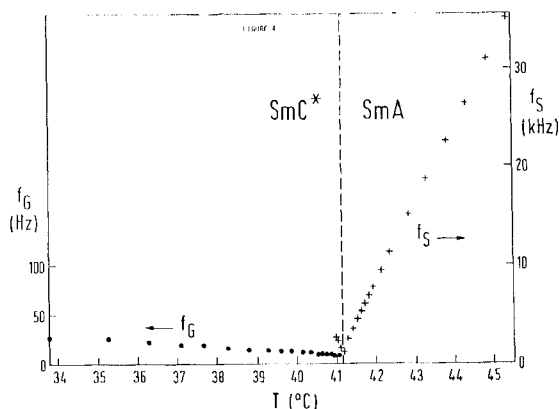


FIGURE 26 Relaxation frequencies for the Goldstone and soft modes.

C and the conductance G of the sample. The C and G values can be transferred by computer and printed with the corresponding values of the dielectric constant ϵ' and ϵ'' using the relations $\epsilon' = C/C_0$ and $\epsilon'' = G/(2\pi f C_0)$ where f is the frequency of the measuring field. For a pure Debye-relaxation (as in e.g. a pure Goldstone or soft-mode relaxation) the frequency dependence of the real and imaginary part of ϵ^* ($\epsilon^* = \epsilon' - j\epsilon''$) are given by⁷⁰

$$\epsilon' = \epsilon_\infty + [\epsilon_0 - \epsilon_\infty]/[1 + (f/f_R)^2] \quad (27)$$

$$\epsilon'' = (f/f_R)[\epsilon_0 - \epsilon_\infty]/[1 + (f/f_R)^2] \quad (28)$$

Typical Debye behavior (with the single relaxation frequencies $f_R = f_G$ and $f_R = f_S$ for the Goldstone-mode and soft-mode, respectively) are clearly seen in the experimental curves in Figure 27. The Goldstone-mode absorption and permittivity curves in Figure 27a are recorded in the smectic C^* phase,⁷¹ while the corresponding soft-mode curves come from the smectic A^* phase.⁶⁹

Measurements of $\epsilon_{||}$, ϵ_{\perp} and $\Delta\epsilon$. For ferroelectric liquid crystals, the dielectric anisotropy $\Delta\epsilon$ ($\epsilon_{||} - \epsilon_{\perp}$) plays an important role in the switching processes and also for dielectric stabilization. Experimentally, to obtain $\Delta\epsilon$, one has to measure both components $\epsilon_{||}$ and ϵ_{\perp} . The experimental set-up that may be used for this purpose is shown in Figure 28. The dielectric studies shown in Figure 24–27 were made using a HP4192 impedance analyser for frequencies between 5 Hz and 13 MHz. The sample cells consist of two conducting glass plates

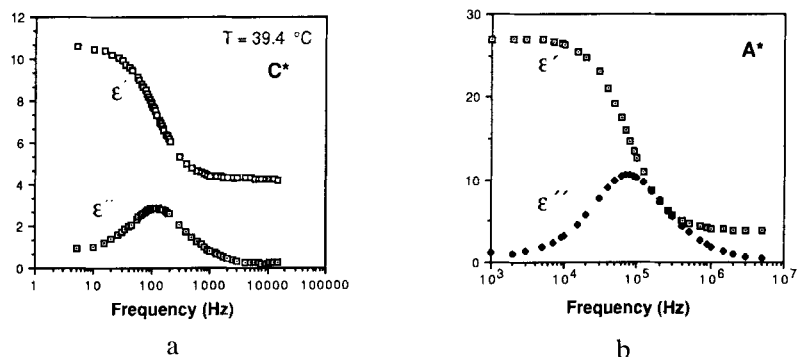
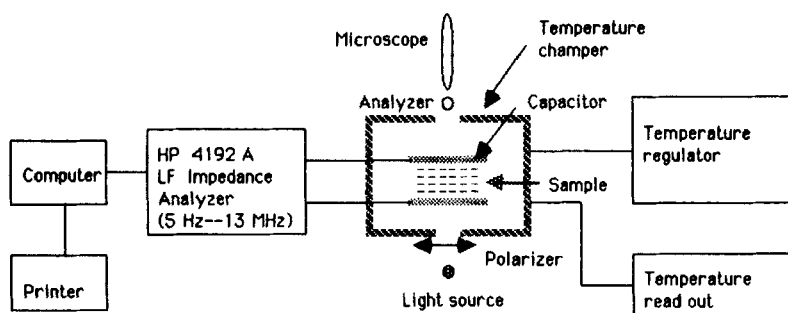


FIGURE 27 Debye-relaxation in the smectic C^* phase (a) and in the smectic A^* phase (b).



Schematic representation of the setup used for dielectric measurements

FIGURE 28 Set-up for dielectric measurements (from Ref. 69).

separated by two mylar spacers with a known thickness. For planar and homeotropic orientations spacers of $100\ \mu\text{m}$ and $50\ \mu\text{m}$ thickness were used. The cell constant C_0 (empty cell capacitance) is measured at room temperature and it is found to be frequency independent in the range 1 kHz to 5 MHz within 1%. For the ϵ_{\perp} measurements, the value of C_0 is measured without any previous surface treatment of the glass plates except washing with acetone. The cell is filled in vacuum with liquid crystal, by capillary effect achieved by heating the sample to the isotropic or to the cholesteric phase if it does exist in the compound under investigation. Later, the cell is placed in a heating stage and the temperature is stabilized using a precision temperature regulator. The alignment for ϵ_{\perp} measurements is assured by placing the temperature chamber containing the sample holder in a magnetic field of 1.2 Tesla as shown in Figure 29a. The sample is slowly cooled from the isotropic phase to the cholesteric phase under magnetic field, and by further cooling towards the cholesteric-smectic A transition, due to the divergence of the cholesteric pitch, a fairly well aligned smectic A phase is observed by simultaneous microscopic observation. The dielectric measurements are performed after removing the cell from the magnet. The measuring electric field is applied perpendicular to the helical axis as shown in Figure 29b.

For ϵ_{\parallel} measurements, the glass plates of the cell are coated with a surfactant to achieve homeotropic orientation. The cell constant C_0 is measured in the presence of the surfactant layer on both surfaces of the capacitor. By observing the filled cell between crossed polarizers, the establishment of homeotropic orientation in the smectic A

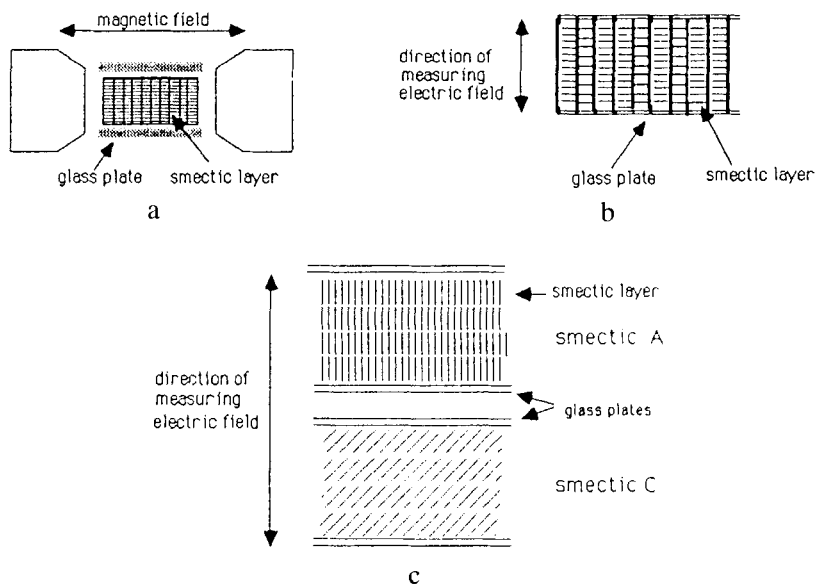


FIGURE 29a. Magnetic field orientation method. *b*. The oriented sample. *c*. Homotropic orientation.

phase is ascertained. The C and G measurements are carried out when the measuring ac field is applied perpendicular to the smectic layers as indicated in Figure 29c. In the C* phase the field is applied perpendicular to the smectic layers and makes an angle (the tilt angle) with the director as shown in the figure.

With the experimental set-up described above many types of dielectric study can be made. Recently, the frequency dependence of $\Delta\epsilon$ were studied for several mixtures.⁷² In Table III results for the

TABLE III

Dielectric anisotropy and dielectric/ferroelectric torque ratio for Chisso 1011 at 25°C (Ref. 72).

Frequency (kHz)	$\Delta\epsilon$	diel.torque/ferroel.torque
10	-2.38	0.70
20	-2.41	0.71
100	-2.42	0.71

Chisso mixture 1011 together with estimations (for field strengths 10 Volts/ μm) of the important ratio between dielectric and ferroelectric director torques are given. The dielectric torque ($1/2\Delta\epsilon\epsilon_0 E^2$) will in the high field region be dominant compared with the ferroelectric torque ($P_s E$) because the former is proportional to the square of the applied electric field. From an application point of view, the ratio between the two torques has to be within a certain limit to ensure matrix multiplexibility.

Thermodynamic Models

Thermodynamic properties of the smectic C^* system are usually described by a phenomenological Landau free energy expansion, the first version given by Meyer.⁷³ The expansion is made in terms of an order parameter reflecting the symmetry properties of the medium. One obvious order parameter choice would thus be the spontaneous polarization \mathbf{P} itself. For a second-order smectic A^* –smectic C^* transition, a Landau expansion involving only \mathbf{P} yields $P \sim (T_{AC} - T)^{1/2}$. However, contrary to the situation for the majority of solid ferroelectrics, experimental evidence show that in the ferroelectric smectics the spontaneous polarization does not provide the drive for the paraelectric–ferroelectric transition. The spontaneous polarization is thus a secondary quantity, since consideration of \mathbf{P} alone is not sufficient to describe all aspects of the transition, *e.g.*, the behavior of the specific heat. In this sense, the ferroelectric smectics could be classified as “improper ferroelectrics.”⁷⁴ As the primary order parameter one might instead choose the two-component tilt vector $\xi = (\xi_1, \xi_2)$ describing the magnitude and the direction of the tilt of the long molecular axis from the normal to the smectic layers. The vector ξ is the projection of the director \mathbf{n} on the smectic planes. For a non-helicoidal structure (as in Figure 3b), and for small tilt angles, this order parameter reduces to simply the smectic tilt angle θ . To account for the helical structure, and also coupling terms between the tilt and polarization referred to as flexoelectric and piezoelectric contributions, the Landau expansion will be more complicated.

By minimization of the Landau free energy expression with respect to the introduced parameters (the tilt angle, polarization and helical pitch) it is possible to obtain the temperature dependences of these parameters. The Landau free energy density describing the SmA –

SmC* transition is usually expressed as⁷⁵

$$\begin{aligned}
 g(z) = & \frac{1}{2}a(\xi_1^2 + \xi_2^2) + \frac{1}{4}b(\xi_1^2 + \xi_2^2)^2 - \Lambda \left(\xi_1 \frac{d\xi_2}{dz} - \xi_2 \frac{d\xi_1}{dz} \right) \\
 & + \frac{1}{2}K_{33} \left[\left(\frac{d\xi_1}{dz} \right)^2 + \left(\frac{d\xi_2}{dz} \right)^2 \right] + \frac{1}{2\chi}(P_x^2 + P_y^2) \\
 & - \mu \left(P_x \frac{d\xi_1}{dz} + P_y \frac{d\xi_2}{dz} \right) + C(P_x \xi_2 - P_y \xi_1)
 \end{aligned} \quad (29)$$

The tilt of a molecule breaks the axial symmetry around its long axis inducing an in-plane polarization $\mathbf{P} = (P_x, P_y)$ perpendicular to the tilt. P_x and P_y are the components of the in-plane polarization, $a = \alpha(T - T_0)$, $b > 0$, K_{33} is the elastic modulus, Λ the coefficient of the Lifshitz term responsible for the twist-bend modulation, μ and C are the coefficients of the “flexo-” and “piezo-” electric coupling between the tilt and the polarization. For small tilt angles θ we may write

$$\xi_1 = n_z n_x \approx \theta \cos \phi; \quad \xi_2 = n_z n_y \approx \theta \sin \phi \quad (30)$$

where $\phi = \phi(z)$ is the azimuthal angle determining the orientation of the molecular direction $\mathbf{n} = (n_x, n_y, n_z)$ with respect to the normal $\mathbf{z} = (0, 0, 1)$ to the smectic layers. With the helicoidal ansatz

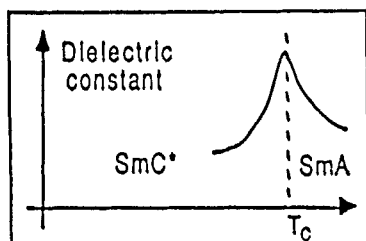
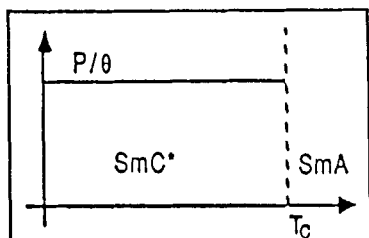
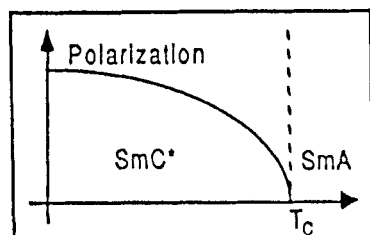
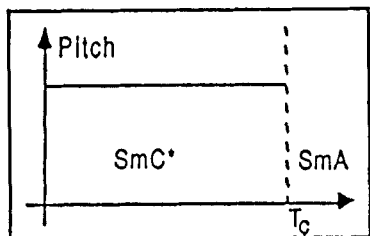
$$\xi_1 = \theta \cos(qz); \quad \xi_2 = \theta \sin(qz) \quad (31)$$

$$P_x = -P \sin(qz); \quad P_y = P \sin(qz) \quad (32)$$

substituted into the expression for $g(z)$ we get

$$\begin{aligned}
 g(z) = & \frac{1}{2}a\theta^2 + \frac{1}{4}b\theta^4 - \Lambda q\theta^2 + \frac{1}{2}K_3 q^2 \theta^2 \\
 & + \frac{1}{2\chi}P^2 - \mu q P \theta - C P \theta \quad (33)
 \end{aligned}$$

Result from $g(z)$ expansion



Experiments

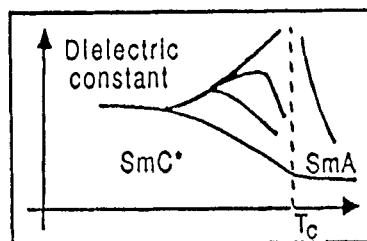
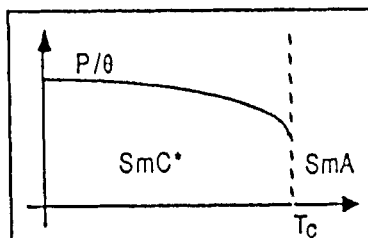
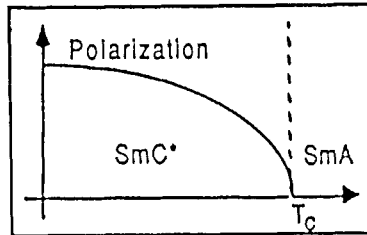
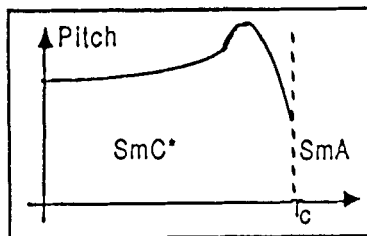


FIGURE 30 Comparison of predictions from the Landau expansion $g(z)$ used above with typical experimental results (from Ref. 5).

Minimization of

$$F = \frac{1}{L} \int_0^L g(z) dz \quad (34)$$

with respect to θ , P and q yields the SmA–SmC* transition temper-

ature T_c , the temperature dependence of the tilt angle and the pitch of the helix as well as the spontaneous polarization P :

$$\theta = \sqrt{\alpha/b} (T_c - T)^{1/2} \quad (35)$$

$$T_c = T_o + \frac{1}{\alpha} [\chi C^2 + (K_{33} - \chi\mu^2) q^2] \quad (36)$$

$$Z = \frac{2\pi}{q} = 2\pi \frac{K_{33} - \chi\mu^2}{\Lambda + \chi\mu C} \quad (37)$$

$$P = \chi(\mu q + C)\theta \quad (38)$$

In this model the pitch of the helix (Z) does not depend on temperature, and the polarization is proportional to the tilt angle. By including a field-term for the interaction with an external electric field in the free energy expression $g(z)$, it is also possible to extract the temperature dependence of the dielectric constant ϵ . In Figure 30 is shown schematically the predictions of the Landau model given above, together with typical experimental results.

The model is insufficient to accurately describe the temperature dependence of the pitch, and also of the dielectric constant. More elaborate models have therefore been suggested recently, adding additional terms in the Landau expansion.⁶⁸

APPLICATIONS

The polar coupling of ferroelectric liquid crystals' (FLCs) large optical anisotropy to applied electric fields is useful for light-modulating devices with the desirable combination of fast, low-voltage, low-power switching properties. This combination of properties is not found in any other electrooptic technologies, ensuring that FLCs will find a place as light modulators. The rapid change of their polarization with temperature near the phase transition makes them also useful as thermoelectric detectors. The large international effort over the past half-dozen years to develop practical devices exploiting FLCs has required the development of a detailed understanding of the physics of FLC devices and the techniques used to fabricate them. We do not intend now to review all this work, but merely to present a simplified view of the principles underlying typical devices, and to

point out how, in comparison to other light modulating technologies, certain applications are best served by FLCs.

Basic Principles: The Idealized SSFLC Device

The simplest structure one can imagine for the smectic C phase is planar layers with a uniform director field. Although recent investigations have shown that the situation in actual devices is rather more complicated, with significant consequences for performance characteristics, many important principles can be most easily understood by considering an idealized device. In this section we describe the basic fabrication requirements and characteristics of surface-stabilized devices having an idealized structure with planar layers perpendicular to the electrode plates. In the next section we describe more realistic device structures, and point out where their performance characteristics will differ from those predicted on the basis of the idealized structures.

Surface stabilization. The change in optic axis direction accompanying the fast director reorientation produced by a change in the externally applied electric field is the mechanism of the electrooptic effect in FLCs. Obtaining this reorientation uncomplicated by the motion of topological defects in the director field requires the suppression of the FLC's intrinsic helix. This can be accomplished without any requirement for an externally applied field by using the method of "surface-stabilization," originated by Clark and Lagerwall.² Figure 31 shows the resulting device geometry. The FLC is bounded by

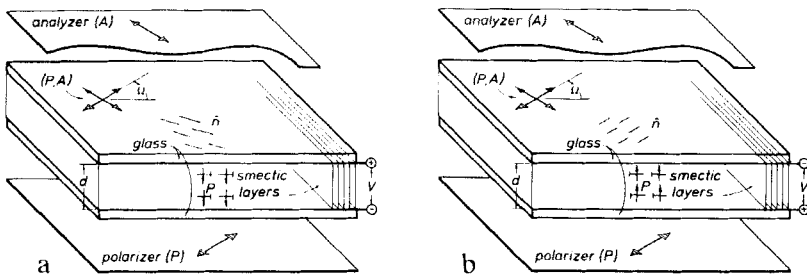


FIGURE 31 Idealized SSFLC device geometry, showing liquid crystal slab of thickness d between glass plates with electrodes on their inner surfaces. The smectic layers are planar and perpendicular to the bounding plates; the director \hat{n} is indicated by a line segment, and the ferroelectric polarization \mathbf{P} by an arrow. State (a) with the director approximately 45° to the polarizer and analyzer transmits light, while state (b) with the director parallel to the polarizer extinguishes.

parallel transparent electrode plates, with the smectic layers oriented at least approximately perpendicular to the plates. If the interaction of the liquid crystal with the plates prefers some director azimuth over others, e.g. it prefers the director parallel to the plates, then the intrinsic helix will become energetically unfavorable when the plate spacing d is small enough. The actual critical spacing depends on the surface anchoring strength which can be characterized by the surface extrapolation length $l_s \equiv K/\gamma$, where K is the bulk Frank elastic constant and γ is the surface energy anisotropy. In the usual case where $l_s \ll d$, the helix is unwound when $\ln d/l_s > qd$, where $q \equiv 2\pi/Z$ is the wavevector of the helix. In fact, l_s is usually comparable to the 30 Å molecular length, so for helix pitch Z in the range of 1 μm, surface stabilization occurs when the plate spacing is comparable to or smaller than Z .

Alignment. To make a useful electrooptic device some means must be employed to align the smectic layers parallel to a common direction so that optic axis orientation of a chosen device state has a uniform projection onto the plates. In the first SSFLC device, this alignment was achieved by a gentle shearing motion of the two electrode plates while the liquid crystal material was heated to its smectic A phase.² Many other alignment techniques which were first demonstrated on thick (helixed) cells will also work. If the FLC has also a smectic A phase it will align upon cooling in a sufficiently large magnetic field.^{37,82} This method has also been demonstrated to work, albeit with difficulty, with surface-stabilized devices.⁸³ Kondo *et al.*⁸⁴ have shown that well-aligned samples can be prepared by nucleating the smectic A phase on a surface at the sample's edge that promotes the desired layer orientation, and then growing the crystal out from the "seed" surface by cooling with a thermal gradient across the sample. Coating the electrode plates with a director-aligning layer similar to those used for nematics,⁸⁵ however, seems to be also the most practical technique for FLCs. Obliquely evaporated films, which were first used with nonchiral smectic C materials,⁸⁶ align FLCs as well.^{38,87,88} Rubbed polymer alignment films,^{89,90} are now perhaps the most commonly used method. The aligning layer techniques work by a straightforward mechanism in FLC materials having a smectic A phase at temperatures immediately above the ferroelectric phase: the director alignment in that phase produces aligned layers which evidently remain fixed in orientation upon cooling of the specimen into the tilted smectic C* phase. The same techniques can also be used with materials having a nematic (N*) phase immediately above the

C* phase, although now the tilt of the smectic layers away from the fixed director potentially introduces a degeneracy^{91,92} which defeats the alignment. This degeneracy can be broken by the application of an electric field with a DC component or by choosing different surface treatments for the two electrode plates.⁹³

Optics. Thus, an FLC prepared between plates spaced closely enough, and aligned e.g. by an anisotropic surface treatment, will have approximately the configuration shown in Figure 31. Opposite voltages applied across the plates select between two orientations of the ferroelectric polarization **P** also nearly perpendicular to the plates. The director orientations corresponding to these field-preferred states are both nearly parallel to the plates, but differ in orientation by nearly twice the smectic C tilt angle θ . Thus, this device is effectively a uniform birefringent waveplate, whose axis can be toggled by reversing the sign of an applied electric field.

It is important to note that in this simplified representation of the SSFLC device, two, and only two, optical states are selected by the applied field. This is in marked contrast to most nematic devices, where only one state can be selected by the applied field, and to obtain any other states one must rely on viscoelastic relaxation to a state preferred by surface interactions. This difference accounts for the speed advantage of the FLC device, since switching from either state to the other can be driven arbitrarily fast by the applied field. The SSFLC device, being effectively binary, also differs significantly from devices exploiting conventional electrooptic materials where their optical response depends in a continuous way on the applied field strength.

The configuration of Figure 31 can be used as a simple intensity modulator by placing the FLC cell between crossed polarizers oriented as shown so that one of the field-preferred optic axis orientations is parallel to either the polarizer or the analyzer. This state would ideally completely extinguish incident light, while the other field-preferred state, having its optic axis orientation intermediate to the axes of the polarizer and analyzer, would transmit light. With the assumption that the layers are in fact perpendicular to the plates so the field-preferred optic axis states are parallel to the plates and differ in orientation by 2θ , the on-axis transmittance is given by:

$$T = \sin^2 4\theta \sin^2(\pi \Delta n d / \lambda). \quad (39)$$

Tilt angles of typical FLC materials with smectic A* to smectic C* phase sequences are between 20° and 25°, which are conveniently

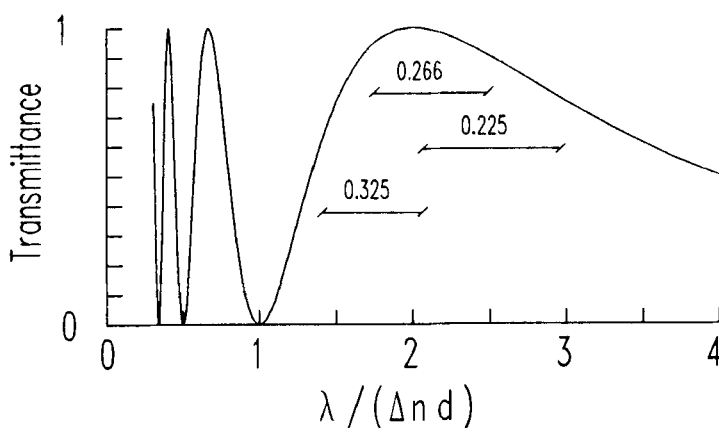


FIGURE 32 Theoretical dependence of transmittance T on $\lambda/\Delta n d$. The bars show the extent of the visible spectrum (450–650 nm) for the indicated values of $\Delta n d$ (in μm). For the optimum value of $\Delta n d = 0.266 \mu\text{m}$, the transmission peaks at 1.0 for $\lambda = 532 \text{ nm}$, and decreases to 0.92 at the extremes of the visible spectrum. [After Lagerwall *et al.* Conference Record of the 1985 International Display Research Conference (IEEE, New York, 1985) p. 213.]

close to the optimum 22.5° . Figure 32 plots the wavelength dependence of equation (39), showing that transmission relatively insensitive to wavelength can be obtained by choosing the device thickness d to place the first-order birefringence maximum at the center of the operating wavelength range. For example, retardances $\Delta n d$ between 250 and 280 nm produce a device that appears “white”. Typical FLC birefringence of 0.15 would then require a device thickness of 1.7 to 1.9 μm , which is quite compatible with the requirements for surface stabilization.

1.2 Realistic SSFLC Device Structures

The configuration with planar layers perpendicular to the plates and uniform director fields is far from the most general one allowed by the symmetries of the smectic C phase and its interactions with its bounding surfaces.

Layer structure. The simple liquid crystal plus surface structures described above are in fact realized in the smectic A phase. The interaction between simple polymer or glass surfaces and the liquid crystal favors the director parallel to the surface, producing, since the smectic A layers must be perpendicular to the director, layers perpendicular to the bounding surfaces. This also effectively requires

that the layers be planar. The tilting of the molecules away from the layer normal upon cooling into the smectic C phase removes the requirement that the layers be perpendicular to the plates, but necessitates the layer spacing be reduced from what it is in the smectic A phase. The actual structure of SSFLC preparations revealed by recent x-ray diffraction studies¹⁹ shows that this layer shrinkage occurs through the formation of the "chevron" layer structure shown in Figure 33. The formation of this structure can be explained by the assumption that the intersection lines of the layer planes with the bounding surfaces are not free to slide along the surface and that the number of layers is conserved at the smectic A to C phase transition (*i.e.* that the layer shrinkage is not accomplished by the introduction of new layers with their attendant layering defects). Thus, the SSFLC layers are typically neither perpendicular to the plates nor planar. The full consequences of this structure for the electrooptics of the SSFLC device can only be understood by considering also the interactions of the director with the bounding surfaces and the chevron "kink" surface.

Director structure. The most symmetric director-surface interactions would favor the director parallel to the surface, but would not

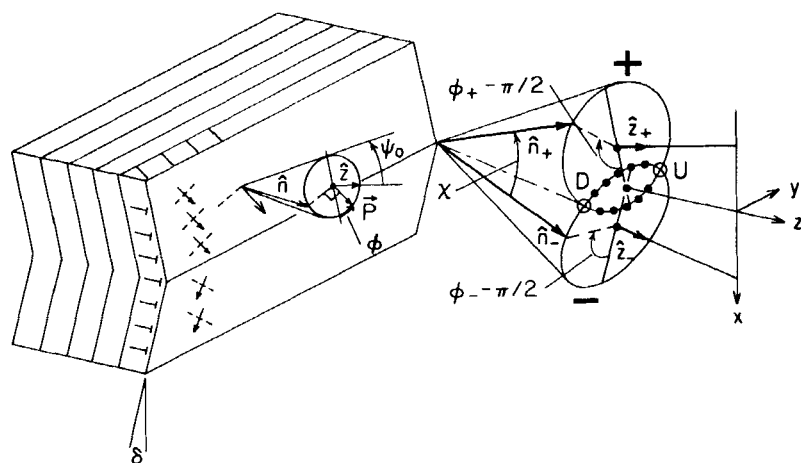


FIGURE 33 Chevron structure with the layers tilted an angle δ away from the bounding plate normal. The director $\hat{n}(r)$ is tilted an angle ψ_0 to the local layer normal $\hat{z}_+(r)$ or $\hat{z}_-(r)$, and is free to reorient in azimuth ϕ . Subscripts $+$ and $-$ refer to quantities respectively above and below the chevron kink. The angle $\chi(\phi_+, \phi_-)$ measures the difference in orientation of directors immediately adjacent on opposite sides of the kink; for $\delta < \theta$, χ can be made zero, and hence director strain across the kink made zero, for the two director states marked U and D in the figure.

distinguish between that orientation with \mathbf{P} pointing out of the FLC into the plates ($\mathbf{P} \cdot \hat{s} > 0$) and that with \mathbf{P} pointing into the FLC ($\mathbf{P} \cdot \hat{s} < 0$). However, the reduced symmetry of the chiral smectic C^* phase allows a lower-order surface interaction that prefers one sign of $\mathbf{P} \cdot \hat{s}$ over the other (\hat{s} is the FLC slab's surface normal unit vector). This arises both from the direct molecular interaction with the surfaces and from the spontaneous bend of the c -director in the smectic C^* phase. In general, the director-surface interactions could favor nonzero tilt of the director away from the surface; the director states stabilized in this case are described in detail by Clark and Lagerwall,⁶ but most of the surface preparations used commonly in the FLC devices studied to date are known to produce nearly zero tilt (at least with nematics), so we will confine our description to that case.

In devices without layer chevrons, prepared for example from a material with no smectic A phase, the polar surface interactions in thick enough devices produce a nonuniform ground-state director structure with splay of \mathbf{P} as shown in Figure 34.⁹⁴ At zero applied field the splay is uniform, *i.e.* the azimuth ϕ of the polarization \mathbf{P} varies linearly as position is varied along the plate normal, as shown in Figure 34(c). Applied fields distort this structure, confining the nonuniformity to within a length $\xi = (K/PE)^{1/2}$ of the surface (K is the effective elastic constant). When the applied field E is strong enough that ξ becomes less than the surface extrapolation length l_s , a discontinuous director reorientation occurs,⁹⁴ leaving the device with a uniform director field. Thus, this device exhibits three distinct states: the splayed state at low and intermediate applied fields, and uniform-polarization UP, Figure 34(a), and DOWN, Figure 34(b), states at high applied fields.

The introduction of the layer chevron adds another surface, at the chevron kink, with which the director interacts. The kink is sharp, having a thickness in a sample with layers spaced by a and tilted away from perpendicular to the plates by an angle δ of about a/δ ,⁹⁵ producing a strong surface with interaction energy of the order $K\delta/a$ comparable to the strength of the solid bounding surface interactions. For layer tilt δ less than the smectic C tilt angle θ there are two azimuths at which the director orientation can be continuous across the kink, as shown in Figure 33, both having the director parallel to the kink plane and hence the bounding plates.⁹⁵ These two azimuths grow progressively closer to each other as δ approaches θ , leaving only one azimuth allowing director continuity across the kink for $\delta = \theta$, and forcing director elastic stress for $\delta > \theta$. Since the director

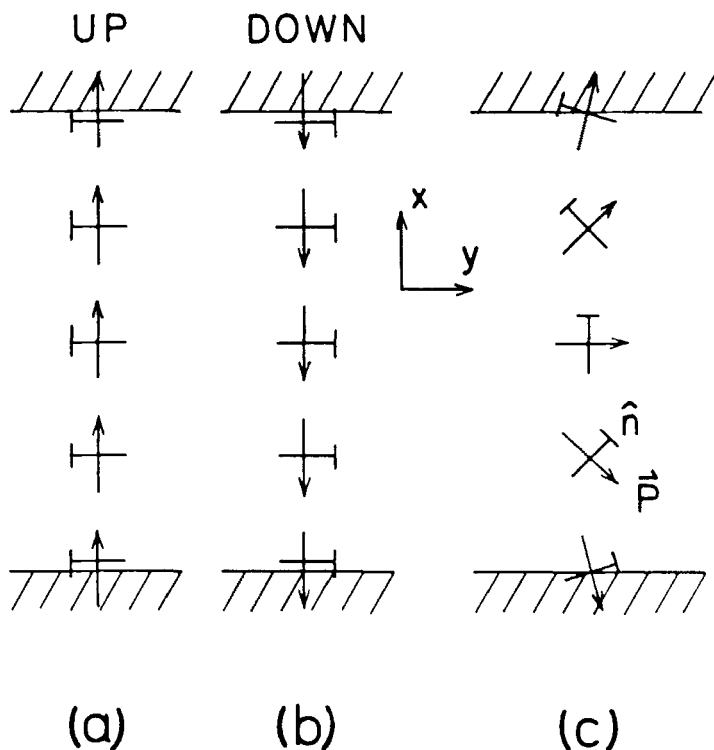


FIGURE 34 Splayed and uniform director structures in SSFLC device with untilted, planar layers and polar surface interactions. The figure is a section in the plane of a smectic layer, the polarization \mathbf{P} shown as an arrow, and the director as a bar with a crossbar on the end projecting out of the page. (a) Uniform state obtained with large UP field; (b) uniform state obtained with large DOWN field; (c) state with splayed polarization obtained at low applied field, here shown with the uniform splay at zero applied field.

is strongly anchored at the kink, the critical spacing for helix unwinding in chevron devices is the spacing from the plate to the kink.

The combination of polar and nonpolar director interactions at the bounding plates with the interactions at the kink surface determines the stable states of the device. The case with appreciably polar surfaces and $\delta < \theta$ produces a device with two energetically equivalent, optically distinct states stable at zero applied field, either of which can be transformed into a uniform state by the application of a sufficiently strong field of the appropriate sign, giving a device with discontinuous switching between four director states,⁹⁶ as shown schematically in Figure 35. This case is frequently observed in experiments with SSFLC preparations on polymer-coated or clean glass surfaces.¹³

If the polar surface interactions were weaker by comparison to the nonpolar ones, or if the device were made thin enough, one could obtain simpler behavior, with the two nearly uniform UP and DOWN states stable in the absence of applied field. However, when the layer tilt δ equals the director tilt θ , a surface that favors the director parallel to itself can stabilize only one state, that state now having polarization parallel to the surface. Thus, the condition $\delta < \theta$ is required for the device to have more than one state stable in the absence of applied field. Recent studies of the glass-FLC interface using the technique of measuring the depolarization of totally internally reflected light show that in fact this surface prefers the director nearly parallel to itself, and that the director within about 100 Å of the surface is reoriented by the discontinuous switching transitions.⁹⁷

Optics. When the applied electric field is so high that ξ is small compared to both the sample thickness d and the incident light's wavelength λ the SSFLC device reduces effectively to two uniform birefringent slabs whose optics are approximately described by equation (39) above if the value of Δn there is suitably reduced according to the tilt of the layers. However, at low applied fields, the director nonuniformities produce significant optical effects. Basically, a device with a nonuniform director orientation will not extinguish transmitted light at any orientation between crossed polarizers. Much can be

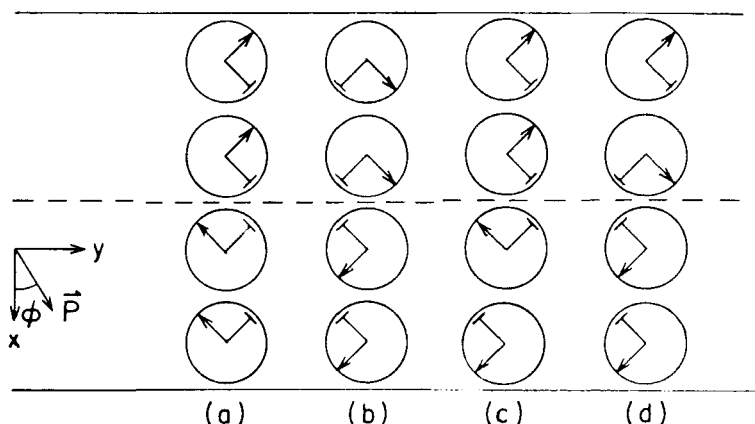


FIGURE 35 Four-state switching. (a) Uniform UP state obtained with large applied field. This is transformed to the SPLAYED/UP state (d) upon removal of the field. Moderate DOWN fields transform state (d) to SPLAYED/DOWN state (c), while still larger DOWN fields give uniform state (b). The arrow indicates polarization \mathbf{P} while the crossbar indicates the c-director.

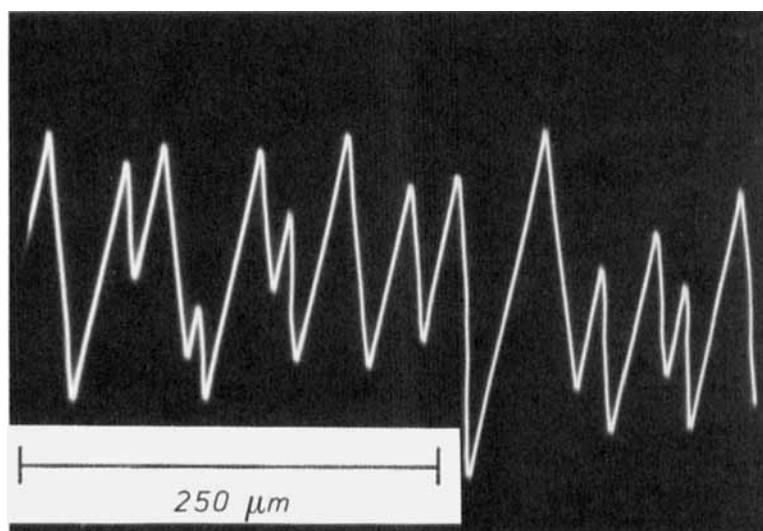


FIGURE 36 Zig-zag wall. Micrograph of SSFLC preparation on rubbed polyvinyl alcohol coated plates. Scale bar below photo shows 250 μm length.

learned about the director structure by measuring the transmittance of such a device as a function of light wavelength.^{96,98} The measured spectra can be fit using transmittances calculated from a model director structure; these experimental measurements and the attendant calculations generally bear out the qualitative features of the various switching states presented above.

The chevron structure has another gross consequence for the optical appearance of SSFLC devices, namely, the occurrence of the characteristic zig-zag wall, an example of which is shown in Figure 36. In devices whose surfaces do not favor tilt of the director away from the plate the chevron vertex can be displaced from the smectic A layer plane in two energetically equivalent directions. The zig-zag wall separates domains of one displacement direction from domains of the other.⁹⁵ As a smectic layer crosses the defect wall, its two oppositely chevroned sections are joined by a parallelogram. When the chevrons have formed from an untilted smectic A phase, and hence have their vertices in the midplane of the device, the parallelogram section of the layer is vertical. Yet to be published calculations of Rieker and Clark show that the zig-zag wall runs at an angle between 0 and about 0.88 to the rubbing direction (smectic A layer normal), while its width in the midplane of the device varies between 1 and 1/2 times the

sample thickness d . Over this same range of directions, the parallelogram normal makes an angle between δ and 2δ to the smectic A layer normal. At high applied fields, where the director is effectively uniform, the projection of the director in the parallelogram onto the plates then differs by this same angle from the projection in the chevron. Typical δ s of about 18° ¹⁹ imply that when the device is oriented between crossed polarizers so the chevron areas extinguish incident light, the core of the zig-zag wall will be oriented between 18° and 36° to the polarizer, and therefore have transmittance between 35% and 90%. The zig-zag defect wall then transmits an amount of light up to nearly $d/4$ per unit wall length. That typical FLC devices with low-tilt polymer alignment preparations exhibit a maximum contrast with white light illumination between their two field-preferred states typically not much than 100:1 indicates a defect density (wall length/device area) of 20 cm^{-1} . Preliminary reports indicate that the formation of zig-zag walls can be suppressed by symmetry-breaking alignment treatments that favor substantial tilt of the director away from the surface.^{99,100}

1.3 Switching Dynamics

Much of the dynamics of the electrooptic response can be understood by solving a simplified equation of motion for the director. When \mathbf{E} is applied parallel to the layers, as would be the case for layers perpendicular to the plates, this equation is:

$$\gamma \partial \phi / \partial t = K \nabla^2 \phi + PE \sin \phi + \frac{\Delta \epsilon}{4\pi} E^2 \sin^2 \theta \sin \phi \cos \phi, \quad (40)$$

where γ is the viscosity opposing changes in azimuthal angle ϕ as discussed previously, K is the elastic constant for distortions of the c-director, θ is the smectic C tilt angle, and $\Delta \epsilon$ is the dielectric anisotropy (cgs units). This equation neglects the variation of $\Delta \epsilon$ with frequency, the anisotropy of the elasticity, flexoelectric polarization, the charge arising from nonuniform polarization, and the variation of tilt angle with applied field. All the neglected effects can produce significant phenomena; nevertheless the above equation (40) accounts for the most important parts of the switching behavior.

Uniform director. The elastic distortions of the director will all have characteristic sizes smaller than the electric field correlation length $\xi \equiv (K/PE)^{1/2}$. When this length is smaller than any of the lengths of interest (*i.e.* cell thickness d or light wavelength λ) equation

(40) can be considerably simplified by omitting the elastic torque term. In this approximation the equation has the analytic solution:

$$\frac{t}{\tau} = \frac{1}{1 - \alpha^2} \left\{ \ln \frac{\tan(\phi/2)}{\tan(\phi_0/2)} = \alpha \ln \left[\frac{(1 + \alpha \cos \phi) \sin \phi_0}{(1 + \alpha \cos \phi_0) \sin \phi} \right] \right\}, \quad (41)$$

where $\tau \equiv \gamma/(PE)$, $\phi_0 \equiv \phi(t = 0)$, and $\alpha \equiv \Delta\epsilon E \sin^2 \theta / (4\pi P)$.¹⁵ In this uniform-director approximation the boundary value problem for the electric field wave of incident light can also be solved exactly,¹⁵ with the resulting transmittance T , for the situation with smectic layers perpendicular to the plates and the polarizer oriented parallel to the director state with $\phi = 0$, having the form:

$$T = \sin^2[2(\theta - \beta)] \sin^2[\pi(n_e - n_o)d/\lambda]. \quad (42)$$

With the relations $\tan \beta = \tan \theta \cos \phi$, $\sin \theta' = \sin \theta \sin \phi$, $n_o = \sqrt{\epsilon_1}$, $n_e = [\epsilon_2(\epsilon_2 + \Delta\epsilon)/(\epsilon_2 + \Delta\epsilon \sin^2 \theta')]$ ^{1/2}, $\Delta\epsilon \equiv \epsilon_3 - \epsilon_2$, where ϵ_i are the principal components of the dielectric tensor, and with the equation (41) giving ϕ as a function of time, the transmittance as a function of time after an electric field reversal can be calculated.

Several conclusions relevant to device characterization can be drawn. The rise time (time for 10% to 90% change in transmittance) is about 1.8τ for all electric fields giving α appreciably less than 1. Only the delay time (time from the application of the electric field to 10% change in T) shows a significant dependence on ϕ_0 , which in a real device is largely determined by surface interactions. For either sign of dielectric anisotropy, the dielectric torques stop homogeneous switching for applied fields giving $\alpha > 1$, in the case of negative $\Delta\epsilon$ by pinning the director to the orientation perpendicular to the applied field, and in the case of positive $\Delta\epsilon$ by causing the switching to occur over an ever decreasing range of angle about $\phi = 90^\circ$ or $\phi = 270^\circ$. Xue *et al.* have extended these calculations to the case where the smectic layers are tilted relative to the plates.¹⁰¹

Nonuniform director. When spatial variation of ϕ is allowed in the above equation of motion (40), its solution becomes much more complicated. When the variation is restricted to be in the form of a plane wave, one analytic solution corresponding to a solitary wave has been found by Schiller *et al.*¹⁰² Generally, one must resort to numerical techniques. These numerical studies show that the polarization \mathbf{P} of FLC device initially oriented at the position of unstable equilibrium in the applied electric field \mathbf{E} , as would be produced by

instantaneously reversing the field applied to the device, can be reoriented by a one-dimensional, solitary wave.^{49,103} However, for the solitary wave to reorient a whole device of dimension d before part of it is reoriented homogeneously requires that the initial deviation of \mathbf{P} from the exact orientation of unstable equilibrium not exceed $e^{-d/\xi}$. Thermal fluctuations, which are neglected in equation (40), have magnitude $\langle \phi^2 \rangle \approx kT/(Ka) \approx 1$, and thus prevent \mathbf{P} from approaching the exact orientation of unstable equilibrium closely enough for solitary waves to be relevant to actual devices.

Domain walls. Of more practical interest are the domain walls whose motion reorients director near the surface at intermediate applied field strengths. For high applied fields ($\xi < l_s$) the surface will be reoriented homogeneously, while for low fields ($\xi > d$) the domain walls are pinned by defects and only incomplete switching occurs. A typical intermediate-field switching sequence begins with the device in the lowest-energy equilibrium state (not necessarily nearly uniform) determined by the applied field strength, the bulk director elasticity, and the surfaces' anchoring energies. This state will have a director orientation field that depends only on position in the direction normal to the plates. Then a step in the applied electric field \mathbf{E} produces some reorientation of the director homogeneous in planes parallel to the plates. This process can be modeled by equation (40) with the need for only one spatial variable; after a time of a few times $\tau \equiv \gamma/(PE)$ the homogeneous process is complete, leaving the director field uniformly in the field-preferred orientation everywhere except within a distance equal to a few times $\xi \equiv [K/(PE)]^{1/2}$ of a surface. At this point most of the optical response is complete. Further homogeneous reorientation at the surface is impeded by the energy barrier between the surface-preferred orientations, and does not take place unless $\xi < l_s$. MacLennan *et al.* have carried out calculations of $\phi(x,t)$ for the bulk *homogeneous* process in a number of cases of practical interest.^{96,103}

The device can continue to reorient *inhomogeneously* by the nucleation of domain walls in the layer of strained director near the surface. While insufficient torque is available at the surface to homogeneously overcome the energy barrier between the surface-preferred orientations, a domain wall provides a way of localizing the region of unfavorable director orientation. The competition of elastic, ferroelectric, and surface torques on the director produce a domain wall with thickness about l_s near the surface expanding to about ξ the same distance away from the surface. The walls move in the direction

that brings the device state to the lowest-energy equilibrium; their velocity can be estimated by equating the viscous dissipation produced by their motion with the energy released by the polarization reversal and relieving of elastic stress in the surface layer.¹⁰⁴

The various stages of the intermediate-field switching process are illustrated schematically in Figure 37, where the device starts out in the state preferred by an UP field. In this state the layer tilts of the chevron structure in combination with the preference of the bounding plate surfaces to the director parallel to themselves produce "pretilts" of the polarization in opposite rotational senses on the two bounding plate surfaces. When the electric field is reversed the directors above and below the chevron then rotate in opposite directions around the tilt cone, leaving a 2π disclination sheet in \mathbf{P} trapped in the device interior,⁹⁵ as was first inferred by Ouichi *et al.*⁹⁸ However, the finite effective director-surface interaction energy at the kink due to the decoupling of director orientations in opposite halves of the chevron⁹⁵

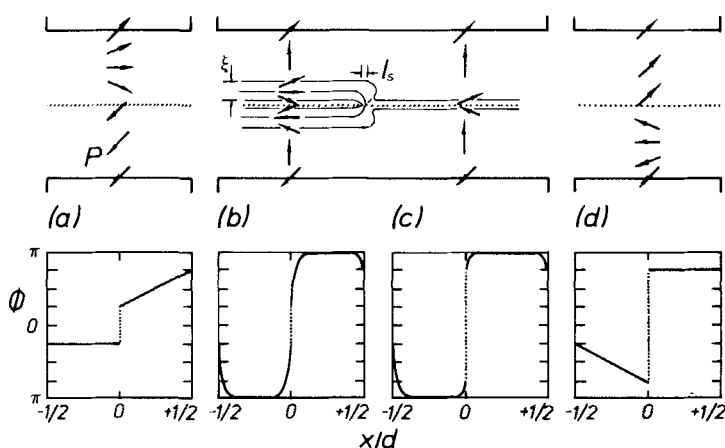


FIGURE 37 Domain walls in chevron cell. (a) shows the initial state of the device: the upper frame shows the polarization \mathbf{P} in a cross section parallel to the smectic A layers. The device is in the SLAYED/ UP state as in Figure 35(d). The lower frame shows the variation of ϕ with position normal to the plates; ϕ is measured as indicated in Figure 35. The dotted line in both top and bottom frames shows the position of the chevron kink; the top plate is at $x = +d/2$. (b) shows the device state at a time $t \approx \tau$ after an electric field step in the $DOWN$ direction has been applied, with a 2π disclination in \mathbf{P} trapped at the chevron kink at $x = 0$. Between (b) and (c) a domain has nucleated and is moving toward (b). After the domain has passed by in (c), the disclination is removed, and the director orientations at the kink have taken up the other orientations parallel to the kink surface. After the field is removed the device takes up the configuration shown in (d), which corresponds to the SPLAYED/ $DOWN$ state of Figure 35(c).

allows a “hole” surrounded by the domain wall to nucleate in this sheet, and expand until the sheet is entirely reoriented. This domain wall may be seen if the device is stroboscopically illuminated, as has been done by Handschy *et al.*,¹⁰⁴ Orihara and Ishibashi¹⁰⁵ and Ouchi *et al.*⁹⁸ Solutions of equation (40) with variation allowed in two dimensions have been calculated by Odamura *et al.*¹⁰⁶ and Yamada *et al.*,¹⁰⁷ showing behavior as described above.

Bistability. Although for applied fields of intermediate strength the domain wall motion contributes only a small part of the optical response, the walls have significant consequences for the final state of the device after the field is removed. If there were no domain wall motion, a relaxation of the strained surface layer would occur with the removal of the applied field, and the device would return to its initial state. However, the domain wall motion switches the director near the surface across an energy barrier that it could not overcome homogeneously, and thus is responsible for switching the device from one stable state to another at fields not so high that $\xi < l_s$.

The phenomena of domain nucleation rate and density, domain wall velocity, and domain coalescence then determine the “latching time” or width of the shortest applied field pulse sufficient to ensure the sample has been switched to a new stable state. The stroboscopic experiments¹⁰⁴ indicate that the domain wall velocity is roughly proportional to applied electric field, in accordance with velocity estimates made by balancing viscous dissipation with the rate at which energy is released as the wall moves. Measurements by Clark and Lagerwall¹⁰⁸ show a latching time dependence approximately proportional to E^{-2} for intermediate fields, indicating a strong dependence of nucleation density or rate on field strength. The stroboscopic experiments also show that nucleation sites, while increasing in density with increasing applied field strength, remain fixed to some perhaps invisible feature in the device rather than occurring at new random locations on each applied field step. A reasonable, but not rigorously verified, hypothesis is that if the field is applied long enough that the domains of reversed surface orientation have coalesced sufficiently to leave unreversed domains with their largest features smaller than some critical size characterized by the sample thickness then the switching will proceed to completion even after the field is removed.

1.4 EXAMPLE APPLICATIONS

Flat panel displays. Currently, the FLC application with the largest commercial potential is the flat panel information display. For

many uses the ubiquitous cathode ray tube (CRT), such as is found in common television receivers, is too bulky and too power consumptive. Nematic liquid crystals (NLCs) have been used to make “nonemissive” displays in the form of very low-profile flat panels, but continue to suffer from undesirably slow switching and poor viewability, particularly when the number of independently addressable picture elements (pixels) is large. In this case some form of multiplexing is required to reduce the number of electronic drivers and connections to a manageable level—the usual method is matrix addressing where a pixel is defined as the overlap of row and column electrodes on the inner surfaces of the liquid crystal cell bounding plates. NLCs’ optical response is to the square of the applied electric field strength averaged over a time comparable to the switching time, which makes it increasingly difficult to differentiate between the effect of the voltage applied to selected pixels and unselected pixels as the number of rows gets large.¹⁰⁹

The bistability and sign-dependence of the FLC’s response makes it possible to devise driving schemes where the voltage pulses applied to an unselected pixel have a very small effect since they alternate in sign and have zero average.¹¹⁰ In this case, the performance of the display is largely independent its number of lines, allowing high-resolution without loss of viewability. These driving schemes write one line (*e.g.* all the every column pixels in one row) in a time a few times the FLC material’s switching time. Thus, the challenge of increasing the number of lines of an FLC display is to decrease the switching time, rather than to sharpen the threshold as in the NLC case. Bone *et al.* have demonstrated the 64 $\mu\text{s}/\text{line}$ switching necessary for European standard 625 line frame, 25 frame/s video.¹¹¹ Figure 38 shows a prototype FLC display with resolution comparable to that of ordinary TV CRTs.

Print heads. Another FLC application of current commercial interest is line-at-a-time image generation on photosensitive media for non-impact printing. Here, a single-line array of FLC light valves is imaged onto the photosensor, which is typically formed into a cylindrical drum. Then, by rotating the drum a high resolution image can be built up line by line. For instance, such an FLC “print head” and a simple illuminator can replace the laser, modulator, and scanner in the electrophotographic laser printer. These printers typically have resolutions of 300 dots/inch (about 12 dots/mm), so the printing of an A4 size page could be accomplished with a print head of about 2500 elements in a 210 mm length equal to the page width. The

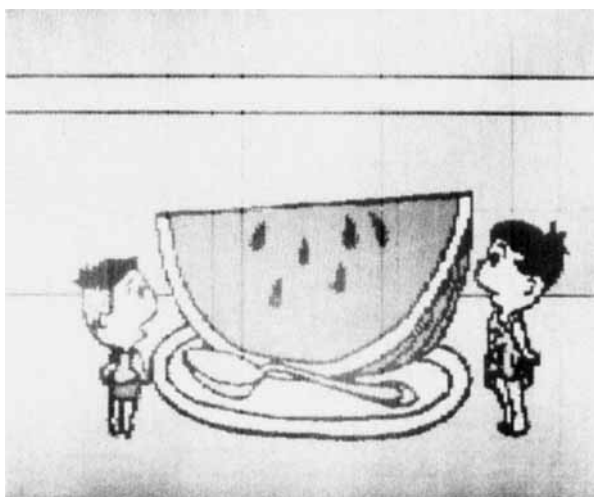
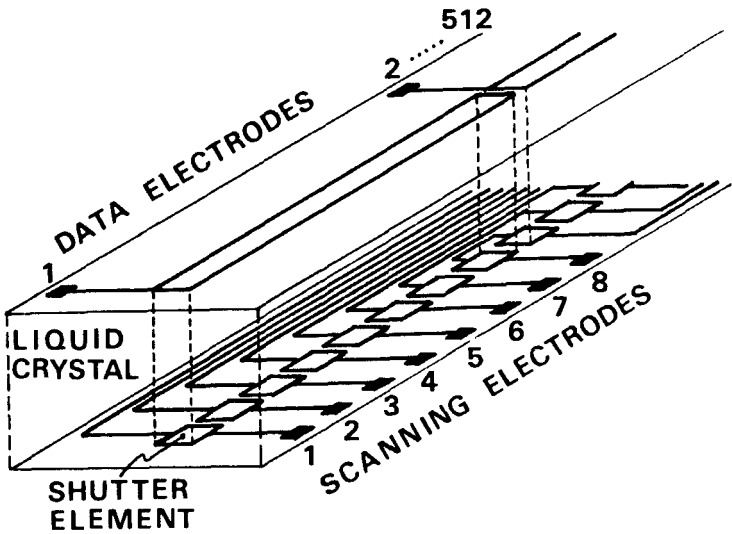


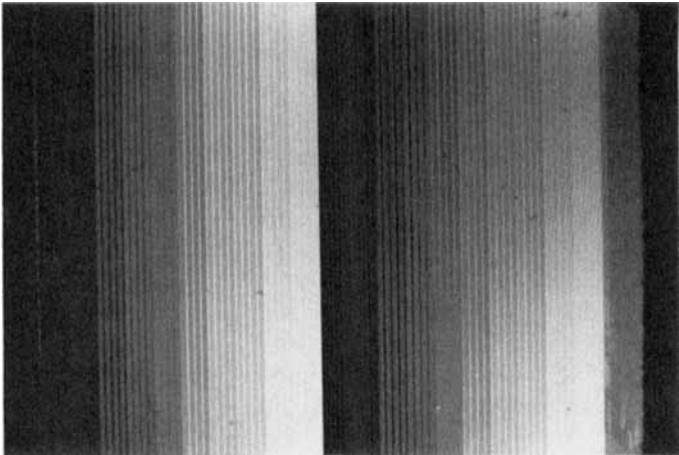
FIGURE 38 Photograph of FLC flat panel display. The panel's active area is 243×182 mm, with 639×400 pixels, and it operates at 30 Hz frame rate. Further description of this prototype is given by its developers [S. Matsumoto, A. Murayama, H. Hatoh, Y. Kinoshita, H. Hirai, M. Ishikawa, and S. Kamagami, 1988 SID International Symposium, Anaheim, California, May 23–27]. Figure courtesy of Toshiba Corporation, Yokohama, Japan. See Color Plate VII.

minimum time to print the page is then a few times the FLC switching time times the number of dots in the page length (about 3600 for the A4 page). With the $30 \mu\text{s}$ switching times of today's faster FLC materials, it should be possible to print with a dwell time per line under $200 \mu\text{s}$ which allows page rates greater than 1/s. In applications not requiring the full speed, matrix multiplexing similar to that described above for displays may be used to reduce the number of electrical connections needed.¹¹² Figure 39 shows a prototype printhead. The high switching speed of the FLC permits the generation of different grey levels in the photosensitive medium's exposure by varying the percentage of the line time a given element is transmitting, as shown in Figure 39(b).¹¹³

Optical computing. The component almost universally needed for optical computing and image processing systems is the spatial light modulator (SLM), which is a device that can impress a two-dimensional modulation pattern or image on the cross section of a light beam. This component bears some similarity to the flat panel display described above. The time required to write a new frame of information is even more critical for optical computing than display ap-



a



b

FIGURE 39 SSFLC print head. (a) "data" electrodes and scanning electrodes are arranged for multiplexing. Figure courtesy of NEC Corporation, Kawasaki-shi, Japan. (b) micrograph of another print head showing individual $200\text{ }\mu\text{m}$ elements with $40\text{ }\mu\text{m}$ gaps between elements. The different apparent transmittances are produced by varying the ratio at the time a given stripe is in the transmitting state (open) to the time it is in the nontransmitting state (closed). For all stripes the open and closed time add to 1 ms.

plications. There are many other light-modulating materials that have been proposed for or demonstrated as SLMs. While many of these other materials have intrinsic switching times much faster than even the future projections for FLCs, in practice the frame rate of most SLMs, including FLC SLMs as we show below, is limited by power dissipation rather than intrinsic switching speed.

All other things being the same, an FLC material with large polarization will switch faster than one with small polarization. However, the energy dissipated in switching a high-polarization material will also be higher than for the low polarization material. In fact, switching a unit area of an SSFLC device by reversing an applied voltage V dissipates an energy $W = 2PV$, ignoring the small reduction of polarization P due layer tilt. Knowing that the 10–90% optical response time t_r is about 1.8τ , where $\tau \equiv \gamma/PE$, the switching energy can be written in terms of t_r as $W = 3.6\gamma d/t_r$, where d is the device thickness. If the switching is repeated every t_r , the power dissipation $U = W/t_r = 3.6\gamma d/t_r^2$. Hence, if the device is limited by the power U it can dissipate, then the fastest achievable switching time is $t_r = [3.6\gamma d/U]^{1/2}$. Assuming that the FLC SLM would operate in reflection, and therefore have a thickness $d \approx 1 \mu\text{m}$, and could dissipate 100 mW/cm^2 without any special cooling system, its switching speed would be limited to $13 \mu\text{s}$ if the FLC material had a viscosity of 50 cP . This speed is comparable to the intrinsic speed of today's best FLC materials. If the dissipation limit could be raised to 10 W/cm^2 , by active cooling systems, the achievable switching time drops to $1.3 \mu\text{s}$. Both the 100 mW/cm^2 and the 10 W/cm^2 performance are better than could be achieved with the intrinsically much faster solid-state electrooptic materials LiNbO_3 or PLZT in an SLM with $10 \mu\text{m}$ pixels.¹¹⁴

Thermoelectric detection. We now briefly describe a final example application where the FLC is used to detect temperature rather than to modulate light. Since FLCs are ferroelectric they are also pyroelectric, meaning that their polarization strength depends on temperature.⁸⁷ This property allows thermal signals to be converted to electric signals. Both surface-stabilized²⁷ and field-unwound⁵⁹ cells have been used, with the detected heat generated by the absorption of light in a thin layer on the bounding plate or in a dye in the FLC itself, respectively. Even previous-generation FLC materials had figures of merit better than conventional solid-state pyroelectrics²⁷; today's state of the art materials could be an order of magnitude better.

Acknowledgments

The authors gratefully acknowledge help provided by the members of the Chalmers and University of Colorado liquid crystal groups, particularly for permission to reproduce illustrations and figures. They thank S. Naemura of the Optoelectronics Research Laboratory of NEC Corp. for providing Figure 39 and S. Matsumoto of Toshiba Corp. for providing Figure 38. This work was supported by the National Swedish Board for Technical Development under Grants No. 84-3691 and No. 84-3638, by the Swedish Work Environment Fund under Grant No. 82-0822 and by the Swedish National Science Research Council under Grant No. 84-3693.

References

1. R. B. Meyer, L. Liébert, L. Strzelecki and P. Keller, *J. Physique (Lett.)*, **36**, L-69 (1975).
2. N. A. Clark and S. T. Lagerwall, *Appl. Phys. Lett.*, **36**, 899 (1980).
3. G. W. Gray and J. W. Goodby, "Smectic Liquid Crystals: Textures and Structures", Leonard-Hill, Glasgow (1984).
4. L. A. Beresnev, V. A. Baikalov, L. M. Blinov, E. P. Pozhidaev and G. V. Purvanetskas, *JETP Lett.*, **33** 536 (1981).
5. S. T. Lagerwall, B. Otterholm and K. Skarp, *Mol. Cryst. Liq. Cryst.*, **152**, 503 (1988).
6. N. A. Clark and S. T. Lagerwall, *Ferroelectrics*, **59**, 25 (1984).
7. V. P. Shibaev, M. V. Kozlovsky, L. A. Beresnev, L. M. Blinov and N. A. Platé, *Polymer Bulletin*, **12**, 299 (1984).
- 8a. P. Pieranski, E. Guyon, P. Keller, *J. Phys. (Paris)*, **36**, 1005 (1975).
- 8b. C. Rosenblatt, R. B. Meyer, R. Pindak, N. A. Clark, *Phys. Rev.*, **A21**, 140 (1980).
9. S. Kai, T. Hashimoto, M. Nomiyama, M. Imasaki, *Jpn. J. Appl. Phys.*, **24**, Supplement 24-3, 52 (1985).
10. S. Kai, T. Hashimoto, M. Nomiyama, M. Imasaki, *Jpn. J. Appl. Phys.*, **24**, Supplement 24-2, 890 (1985).
11. M. E. Lines, A. M. Glass, "Principles and Applications of Ferroelectrics and Related Phenomena," Oxford University Press (1978).
12. R. Williams, G. Heilmeyer, *J. Chem. Phys.*, **44**, 638 (1966).
13. M. A. Handschy, N. A. Clark, *Ferroelectrics*, **59**, 69 (1984).
14. M. Odamura, S. Nonaka, K. Kondo, M. Isogai and K. Anjyo, *Proceedings of the SID Meeting in San Diego*, 1985, p. 228.
15. Xue Jiu-Zhi, M. A. Handschy and N. A. Clark, *Ferroelectrics*, **73**, 305 (1987).
16. I. Dahl, S. T. Lagerwall and K. Skarp, *Phys. Rev. A*, **36**, 4380 (1987).
17. P. Schiller, *Cryst. Res. Technol.*, **21**, 301 (1986).
18. T. Geelhaar, C. Escher and E. Böhm, *17. Freiburger Arbeitstagung Flüssigkristalle*, 1987.
19. T. P. Rieker, N. A. Clark, G. S. Smith, D. S. Parmar, E. B. Sirota and C. R. Safinya, *Phys. Rev. Lett.*, **59**, 2658 (1987).
20. C. B. Sawyer and C. H. Tower, *Phys. Rev.*, **35**, 269 (1930).
21. K. Skarp and G. Andersson, *Ferroelectrics*, **6**, 67 (1986).
22. W. J. Merz, *Phys. Rev.*, **95**, 690 (1954).
23. Ph. Martinot-Lagarde, *J. Physique (Lett.)*, **38**, 17 (1977).
24. K. Skarp, I. Dahl, S. T. Lagerwall and B. Stebler, *Mol. Cryst. Liq. Cryst.*, **114**, 283 (1984).

25. K. Miyasato, S. Abe, H. Takezoe, A. Fukuda and E. Kuze, *Jpn. J. Appl. Phys.*, **22**, L661 (1983).
26. L. M. Blinov, L. A. Beresnev, N. M. Shtykov and Z. M. Elashvili, *J. Physique*, **40**, C3-269 (1979).
27. A. M. Glass, J. S. Patel, J. W. Goodby, D. H. Olson and J. M. Geary, *J. Appl. Phys.*, **60**, 2778 (1986).
28. G. Andersson, I. Dahl, P. Keller, W. Kuczynski, S. T. Lagerwall, K. Skarp and B. Stebler, *Appl. Phys. Lett.*, **51**, 640 (1987).
29. S. Garoff and R. B. Meyer, *Phys. Rev. Lett.*, **38**, 848 (1977).
30. G. Andersson, I. Dahl, P. Keller, W. Kuczynski, S. T. Lagerwall, K. Skarp and B. Stebler, presented at the 1st International Symposium on Ferroelectric Liquid Crystals, Arcachon 1987, to be published in *Ferroelectrics*.
31. B. Otterholm, C. Alstermark, K. Flatischler, A. Dahlgren, S. T. Lagerwall and K. Skarp, *Mol. Cryst. Liq. Cryst.*, **146**, 189 (1987).
32. A. M. Biradar, S. S. Bawa, S. B. Samanta and S. Chandra, *Phys. Stat. Solidi (a)* **97**, 427 (1986).
33. K. Kondo, Y. Sato, H. Takezoe, A. Fukuda and E. Kuze, *Jpn. J. Appl. Phys.*, **20**, L871 (1981).
34. K. Kondo, H. Takezoe, A. Fukuda and E. Kuze, *Jpn. J. Appl. Phys.*, **21**, 224 (1982).
35. K. Kondo, A. Fukuda and E. Kuze, *Jpn. J. Appl. Phys.*, **20**, 1779 (1981).
36. K. Kondo, F. Kobayashi, H. Takezoe, A. Fukuda and E. Kuze, *Jpn. J. Appl. Phys.*, **19**, 2293 (1980).
37. K. Kondo, F. Kobayashi, A. Fukuda and E. Kuze, *Jpn. J. Appl. Phys.*, **20**, 1773 (1981).
38. Ph. Martinot-Lagarde, *J. Physique*, **37**, C3-129 (1976).
39. Ph. Martinot-Lagarde, R. Duke and G. Durand, *Mol. Cryst. Liq. Cryst.*, **75**, 249 (1981).
40. S. A. Rozanski, *Phys. Stat. Sol. (a)*, **79**, 309 (1983).
41. K. Terashima, M. Ichihashi, M. Kikuchi, K. Furukawa and T. Inukai, *Mol. Cryst. Liq. Cryst.*, **141**, 237 (1986).
42. T. Uemoto, K. Yoshino and Y. Inuishi, *Mol. Cryst. Liq. Cryst.*, **67**, 137 (1981).
43. W. Kuczynski, S. T. Lagerwall and B. Stebler, to be published.
44. H. Takezoe, K. Kondo, A. Fukuda and E. Kuze, *Jpn. J. Appl. Phys.*, **21**, L627 (1982).
45. K. Skarp, K. Flatischler, K. Kondo, Y. Sato, K. Miyasato, H. Takezoe, A. Fukuda and E. Kuze, *Jpn. J. Appl. Phys.*, **22**, 566 (1983).
46. P. G. Amaya, M. A. Handschy and N. A. Clark, *Optical Engineering*, **23**, 261 (1984).
47. L. M. Blinov and L. A. Beresnev, *Sov. Phys. Usp.*, **27**, 92 (1985).
48. W. Kuczynski, *Ber. Bunsenges. Phys. Chem.*, **85**, 234 (1981).
49. J. E. MacLennan, M. A. Handschy and N. A. Clark, *Phys. Rev. A*, **34**, 3554 (1986).
- 50a. N. Éber, L. Bata and A. Jakli, *Mol. Cryst. Liq. Cryst.*, **142**, 15 (1987).
- 50b. H. R. Brand and H. Pleiner, *J. Phys. (Paris)*, **45**, 563 (1984).
51. A. C. Diogo and A. F. Martins, *Liquid Crystals of One and Two Dimensional Order* (Eds. W. Helfrich and G. Heppke, Springer Verlag, Berlin, 1980), p. 108.
52. F. J. Bock, H. Knepe and F. Schneider, *Liquid Crystals*, **1**, 239 (1986).
53. E. P. Pozhidayev, L. M. Blinov, L. A. Beresnev and V. V. Belyayev, *Mol. Cryst. Liq. Cryst.*, **124**, 359 (1985).
54. P. Schiller, *Wiss. Z. Univ. Halle XXXIV'85M*, **3**, 61 (1985).
55. P. G. de Gennes, *The Physics of Liquid Crystals*, p. 163 (Oxford University Press, 1974).
56. S. Meiboom and R. C. Hewitt, *Phys. Rev. Lett.*, **34**, 1146 (1975).
57. P. Pieranski, E. Guyon and P. Keller, *J. Physique*, **36**, 1005 (1975).
58. P. Pieranski, E. Guyon, P. Keller, L. Liébert, W. Kuczynski and P. Pieranski, *Mol. Cryst. Liq. Cryst.*, **38**, 275 (1977).

59. See e.g. L. A. Beresnev and L. M. Blinov, *Ferroelectrics*, **33**, 129 (1981).
60. E. P. Pozhidayev, L. M. Blinov, L. A. Beresnev and V. V. Belyayev, *Mol. Cryst. Liq. Cryst.*, **124**, 359 (1985).
61. M. I. Barnik, V. A. Baikalov, V. G. Chigrinov, E. P. Pozhidaev, *Mol. Cryst. Liq. Cryst.*, **143**, 101 (1987).
62. Xue Jiu-Zhi, M. A. Handschy and N. A. Clark, *Liquid Crystals*, **2**, 707 (1987).
63. C. C. Huang, *Mol. Cryst. Liq. Cryst.*, **144**, 1 (1987).
64. W. H. de Jeu, W. J. A. Gossens and P. Bordwijk, *J. Chem. Phys.*, **61**, 1985 (1974).
65. L. Benguigui, *J. Phys.*, **40**, 705 (1979).
66. S. A. Pikin and V. L. Indenbom, *Uspekhi Fiz. Nauk*, **125**, 251 (1978).
67. Ph. Martinot-Lagarde and G. Durand, *J. Phys. Lett.*, **41**, L43 (1980).
68. B. Zeks, *Mol. Cryst. Liq. Cryst.*, **114**, 259 (1984).
69. C. Filipic, T. Carlsson, A. Levstik, B. Zeks, R. Blinc, F. Gouda, S. T. Lagerwall and K. Skarp, *Phys. Rev. B*, (in press).
70. See e.g. C. J. F. Böttcher, "Theory of Electric Polarization," p. 349, Elsevier Publishing Company (1952).
71. R. Eidenschink, T. Geelhaar, G. Andersson, A. Dahlgren, K. Flatischler, F. Gouda, S. T. Lagerwall and K. Skarp, presented at the 1st International Symposium on Ferroelectric Liquid Crystals, Arcachon 1987, to be published in *Ferroelectrics*.
72. F. Gouda, G. Andersson, T. Matuszczyk, K. Skarp, S. T. Lagerwall and B. Stebler, presented at the 1st International Symposium on Ferroelectric Liquid Crystals, Arcachon 1987, to be published in *Ferroelectrics*.
73. R. B. Meyer, *Mol. Cryst. Liq. Cryst.*, **40**, 33 (1977).
74. V. Dvorak, *J. Phys. Soc. Jap. Suppl.*, **28**, 252 (1970).
75. R. Blinc and B. Zeks, *Phys. Rev. A*, **18**, 740 (1978).
76. M. V. Loseva, B. I. Ostrovskii, A. Z. Rabinovich, A. S. Sonin, B. A. Strukov and N. I. Chernova, *JETP(Lett.)*, **28**, 374 (1978).
77. SEIKO Newsletter July 12 (1985).
78. D. M. Walba, S. C. Slater, W. N. Thurmes, N. A. Clark, M. A. Handschy and F. Supon, *J. Am. Chem. Soc.*, **108**, 5210 (1986).
79. D. M. Walba, R. T. Vohra, N. A. Clark, M. A. Handschy, J. Xue, D. S. Parmar, S. T. Lagerwall and K. Skarp, *J. Am. Chem. Soc.*, **108**, 7424 (1986).
80. T. Sakurai, N. Mikami, R. Higuchi, M. Honma, M. Osaki and K. Yoshino, *J. Chem. Soc. Chem. Commun.*, 978 (1986).
81. T. Geelhaar, presented at the 1st International Symposium on Ferroelectric Liquid Crystals, Arcachon 1987, to be published in *Ferroelectrics*.
82. I. Musevic, B. Zeks, R. Blinc, Th. Raising and P. Wyder, *Phys. Rev. Lett.*, **48**, 192 (1982).
83. Katsumi Kondo, Yuzuru Sato, Keita Miyasato, Hideo Takazoe, Atsuo Fukuda, Eiichi Kuze, Kurt Flatischler and Kent Skarp, *Jpn. J. Appl. Phys.*, **22**, L13 (1983).
84. Katsumi Kondo, Hideo Takazoe, Atsuo Fukuda and Eiichi Kuze, *Jpn. J. Appl. Phys.*, **22**, L85 (1983).
85. Jaques Cognard, *Alignment of Nematic Liquid Crystals and Their Mixtures* (Gordon and Breach, New York, 1982).
86. W. Urbach, M. Boix and E. Guyon, *Appl. Phys. Lett.*, **25**, 479 (1974).
87. L. J. Yu, H. Lee, C. S. Bak and M. M. Labes, *Phys. Rev. Lett.*, **36**, 388 (1976).
88. Katsumi Yoshino, K. G. Balakrishnan, Tsutomu Uemoto, Yawuro Iwasaki and Yoshio Inuishi, *Jpn. J. Appl. Phys.*, **17**, 597 (1978).
89. Thomas E. Lockhart, David W. Allender, Edward Gelerinter and David L. Johnson, *Phys. Rev. A* **20**, 1655 (1979).
90. J. S. Patel, T. M. Leslie and J. W. Goodby, *Ferroelectrics*, **59**, 137 (1984).
91. M. Petrov, A. M. Levelut and G. Durand, *Mol. Cryst. Liq. Cryst.*, **82**, 221 (1982).

92. M. Lefevre, J. L. Martinand, G. Durand and M. Veyssie, *C. R. Hebd. Sean. Acad. Sci.*, **273B**, 403 (1971).
93. J. S. Patel and J. W. Goodby, *J. Appl. Phys.*, **59**, 2355 (1986).
94. M. A. Handschy, N. A. Clark and S. T. Lagerwall, *Phys. Rev. Lett.*, **51**, 471 (1983).
95. N. A. Clark and T. P. Rieker, *Phys. Rev.*, **A37**, 1053 (1988).
96. Joseph E. MacLennan, Ph.D. thesis, University of Colorado, Boulder, Colorado, unpublished (1988).
97. J. Z. Xue and N. A. Clark, to be published (1988).
98. Y. Ouchi, H. Takazoe and A. Fukuda, *Jpn. J. Appl. Phys.*, **26**, 1 (1984).
99. Tsuyoshi Uemura, Noriko Ohba, Naohide Wakita, Hiroyuki Ohnishi and Isato Ota, *Proc. SID*, **28**, 175 (1987).
100. Phil Bos and Rickey Koehler/Beran, *Ferroelectrics*, to appear (1988).
101. Xue Jiu-zhi, M. A. Handschy and N. A. Clark, *Liq. Cryst.*, **2**, 707 (1987).
102. P. Schiller, G. Pelzl and D. Demus, *Liquid Crystals*, **2**, 21 (1987).
103. Joseph E. MacLennan, Noel A. Clark and Mark A. Handschy, "Solitary Waves in Ferroelectric Liquid Crystals," in *Solitons in Liquid Crystals*, J. Prost and Lin Lei, editors (Springer-Verlag, to be published 1988).
104. M. A. Handschy and N. A. Clark, *Appl. Phys. Lett.*, **41**, 39 (1982).
105. Hiroshi Orihara and Yoshihiro Ishibashi, *Jpn. J. Appl. Phys.*, **23**, 1274 (1984).
106. Motomi Odamura, Shiro Nonaka, Katsumi Kondo, Masato Isogai and Ken'ichi Anjyo, *Conference Record of the 1985 International Display Research Conference* (IEEE, New York, 1985) p. 228.
107. Y. Yamada, T. Tsuji, N. Yamamoto, M. Yamawaki, H. Orihara and Y. Ishibashi, 11th International Liquid Crystal Conference, Berkeley, California, July 1986.
108. M. A. Handschy, N. A. Clark and S. T. Lagerwall, *Mol. Cryst. Liq. Cryst.*, **94**, 213 (1983).
109. P. M. Alt and P. Pleshko, *IEEE Trans. Electron. Dev.* **ED21**, 146 (1974).
110. J. Wahl, T. Matuszczyk and S. T. Lagerwall, *Mol. Cryst. Liq. Cryst.*, **146**, 143 (1987).
111. M. F. Bone, D. Coates, W. A. Crossland, P. Gunn and P. W. Ross, *Displays* **8**, 115 (1987).
112. S. Naemura, H. Ichinose, H. Kitayama, S. Ishizaki, K. Ohsawa and C. Tani, *Proc. SID*, **28**, 311 (1987).
113. K. Karp, M. Matuszczyk, T. Matuszczyk, B. Bijlenga, Å. Hörnell, B. Stebler and S. T. Lagerwall, presented at the First International Symposium on Ferroelectric Liquid Crystals, Arcachon, France, September 1987; *Ferroelectrics*, to appear (1988).
114. M. A. Handschy, K. M. Johnson, G. Moddel and L. A. Pagano-Stauffer, *Ferroelectrics*, to be published (1988).
115. L. A. Beresnev and L. M. Blinov, *Ferroelectrics*, **33**, 129 (1981).